Bithiazole an Intriguing Electron Deficient Building for Plastic Electronic Applications

Haw-Lih Su,[1] Dusan N. Sredojevic,[1] Hugo Bronstein,[2] Tobin J. Marks,[3,4]

Bob C. Schroeder*[5] and Mohammed Al-Hashimi*[1]

[1] Department of Chemistry, Texas A&M University at Qatar, P.O. Box 23874, Doha, Qatar.

[2] Department of Chemistry, University College London, Christopher Ingold Building, London, WC1H 0AJ, U.K.

[3] Department of Chemical Engineering, Texas A&M University at Qatar, P.O. Box 23874, Doha, Qatar.

[4] Department of Chemistry, Materials Research Center, and Argonne-Northwestern Solar Energy Research Center, Northwestern University, 2145 Sheridan Road, Evanston, Illinois 60208, United States.

[5] Materials Research Institute and School of Biological and Chemical Sciences, Queen Mary University London, Mile End Road, London E1 4NS, U.K.

* E-mail: b.c.schroeder@qmul.ac.uk ; mohammed.al-hashimi@qatar.tamu.edu

Keywords: bithiazole based polymers**,** π-conjugated materials, acceptor building blocks, organic field effect transistors (OFET), organic photovoltaics (OPV).

Abstract:

The heterocyclic thiazole unit has been extensively used as electron deficient building block in π-conjugated materials over the last decade. Its incorporation into organic semiconducting materials is particularly interesting due to its structural resemblance to the more commonly used thiophene building block, thus allowing to tune the opto-electronic properties of a material without significantly perturbing its molecular structure. In this comprehensive review, we discuss the structural differences between thiazole and thiophene based organic semiconductors, and the effects on the physical properties of the materials. We provide the reader with an overview of thiazole based polymers that have emerged over the past decade for organic electronic applications and discuss how the incorporation of thiazole has effected the device performance of organic solar cells and organic field effect transistors. Finally, we conclude with an outlook on how thiazole

based polymers could be incorporated into all-electron deficient polymers, thus, in order to obtain high performance acceptor polymers for use in bulk heterojunction solar cells and as organic field effect transistors. Computational methods were used to discuss some newly designed acceptor building blocks that have the potential to be polymerized with fused bithiazole moiety, hence, propelling the advancement of air stable n-type organic semiconductors.

Introduction

Since the discovery of electrically conducting polymers in the late 1980's, the field of π-conjugated polymers has come a long way. Whereas initially the materials were regarded as a purely scientific curiosity, they have advanced since into a highly interdisciplinary research field, now challenging conventional inorganic semiconductor technologies for market share. Organic semiconductors (OSC) in comparison to their inorganic counterparts, are still struggling to achieve comparable device performances and lifetimes, but are making up for these shortcomings by various other means. Firstly, the chemical and physical properties of organic semiconductors can easily be tuned during the synthesis, allowing for an unprecedented catalogue of semiconducting materials to choose from. Furthermore, OSC are solution processable, which makes them particularly attractive for large area applications using conventional coating techniques, *i.e.* roll-to-roll, slot-die coating or inkjet printing, thus, reducing device fabrication costs. In addition, inorganic semiconductors are largely limited to solid substrates due to their inherent crystallinity, OSC on the other hand can be deposited on flexible substrates, making conformal and stretchable devices no longer only a science fiction vision.

In order to achieve this unparalleled variety of distinctive properties in OSC materials, chemists, physicists and material scientists have worked tirelessly over the last two decades to get a detailed understanding of the structure-property relationships governing the device performances in optoelectronic devices, such as organic field effect transistors (OFET) and organic photovoltaics (OPV).

Organic field effect transistors

A transistor is a semiconducting device used for electric signal amplification, control and generation. To date, both small molecules and polymeric materials have been successfully utilized as semiconducting materials in OFET devices. In a field effect transistor, this modulation is achieved via the application of an electric field causing the accumulation and flow of charges between the electrodes. A typical bottom-gate/top-contact transistor structure is depicted in Figure 1. An OFET transistor consists of three different modules (1) a dielectric layer (SiO_2 in this example) insulating the gate electrode; (2) an organic semiconductor acting as the variable conductance element; and (3) a conductor functioning as the gate, source, and drain electrodes.[1] Source and drain electrodes inject and extract charges from the transistor channel. The gate electrode on the other hand controls the charge density in the channel area at the dielectric-semiconductor interface. It is only when an electrical potential is applied between the gate and the source/drain contacts that charges can accumulate in the channel before being extracted. It is noteworthy that in the transistor device depicted in Figure 1, the current flows from the source to the drain, parallel to the gate electrode plane. The electrodes in OFET transistors are typically metal electrodes (e.g. gold, silver, calcium, silver, etc.) deposited via evaporation through a shadow mask. More recently independent of what type of electrode is used, it is crucial to adjust the work functions of the electrodes to the energy levels of the semiconductor in order to avoid injection and extraction barriers. One popular approach is to functionalize the electrodes with self-assembling monolayers (SAM), which allows the introduction of dipoles at the interface, thus, shifting the effective work function of the metal. In OFET, both molecular and polymeric semiconductors have been successfully employed and in some cases the measured mobilities are comparable to amorphous silicon.
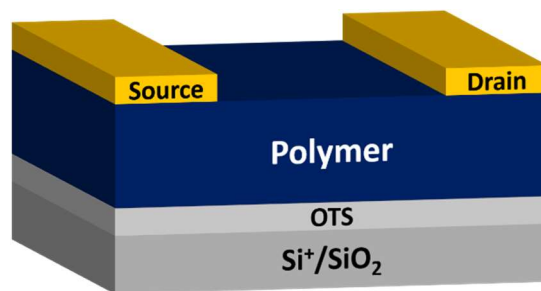

Figure 1. Schematic representation of a bottom-gate/top-contact OFET structure comprising a self-assembled monolayer of octadecyltrichlorosilane (OTS) on the SiO_2 gate dielectric.

Organic photovoltaic cells

A conventionnal organic solar cell consists of a transparent electrode, usually indium tin oxide (ITO) deposited on glass. To smoothen the ITO surface and facilitate hole extraction poly(3,4-ethylenedioxythiophene) polystyrene sulfonate (PEDOT:PSS) is often used as hole transporting layer. Similarly, electron extraction layers are applied to align the energy levels between the active layer and the cathode, thus improving electron extraction and preventing charge recombination. Low work function cathodes (e.g. calcium, aluminium, magnesium) have to be used in conventional device architectures, leading to poor device lifetimes due to the oxidation of the cathode. In most organic solar cells the active layer is based on a bulk heterojunction (BHJ), comprising a blend of electron donor (a small molecule or polymer p-type semiconductor) and an electron accepting fullerene based on a n-type semiconductor (such as [6,6]-phenyl-C_{61}- or C_{71}-butyric acid methyl ester ($PC_{61}BM$ or $PC_{71}BM$)). These are typically produced by depositing a solution of both donor and acceptor and allowing the two components to separate into an interpenetrating bicontinuous layer of donor and acceptor rich regions. An ideal BHJ layer morphology is one which allows all the incident photons to be absorbed and for the resulting exciton to be able to reach a heterojunction before it decays back to its ground state. [2, 3] Finally, the regions of donor and acceptor must contain percolating pathways back to the appropriate electrodes allowing for charge extraction to occur. The typical device architecture is shown in Figure 2 alongside the most commonly used donor polymer poly(3-hexylthiophene) (P3HT) and acceptor $PC_{61}BM$.
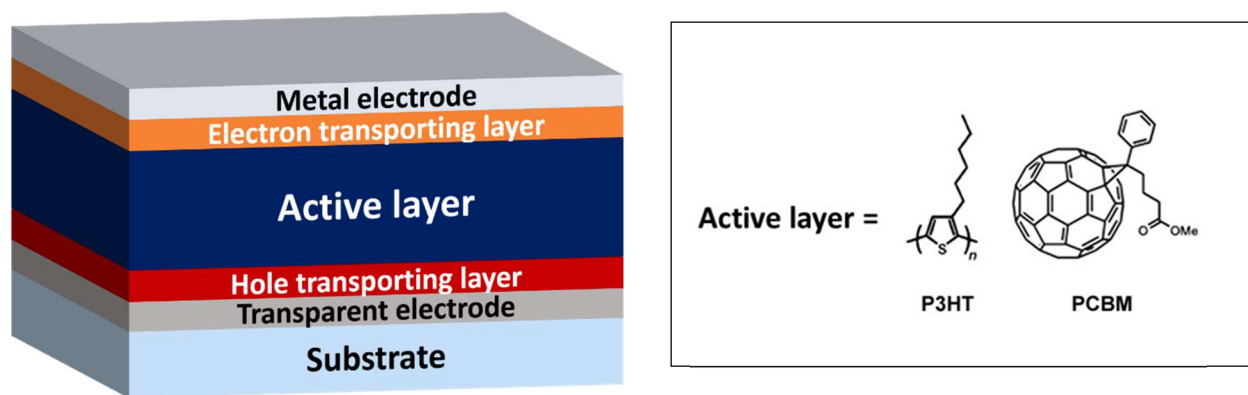

Figure 2. Schematic representation of a conventional BHJ organic solar cell architecture and polymer poly(3-hexylthiophene) (P3HT) and acceptor PC61BM.

In order to obtain the maximum possible efficiency in an OPV device, the donor and acceptor must possess certain electronic characteristics. The overall power conversion efficiency (PCE) of the cell is dictated by three parameters, the short circuit current (J_{sc}), the open circuit voltage (V_{oc}), and the fill factor (*FF*). Assuming an optimal BHJ morphology, the J_{sc} is controlled by the amount of photons the solar cell can absorb and the extent to which these photons are successfully spilt into free charges that do not recombine. Efficient charge separation is encouraged by having a sufficient energetic offset between the lowest unoccupied molecular orbitals (LUMO) of the donor and the acceptor. The V_{oc} is primarily dictated by the energetic difference between the highest occupied molecular orbital (HOMO) of the donor and the LUMO of the acceptor as depicted in Figure 3. Finally, the *FF* is generally a measure of how well the solar cell is performing, *i.e* the charge collection efficiency at low electric fields.[4-6]
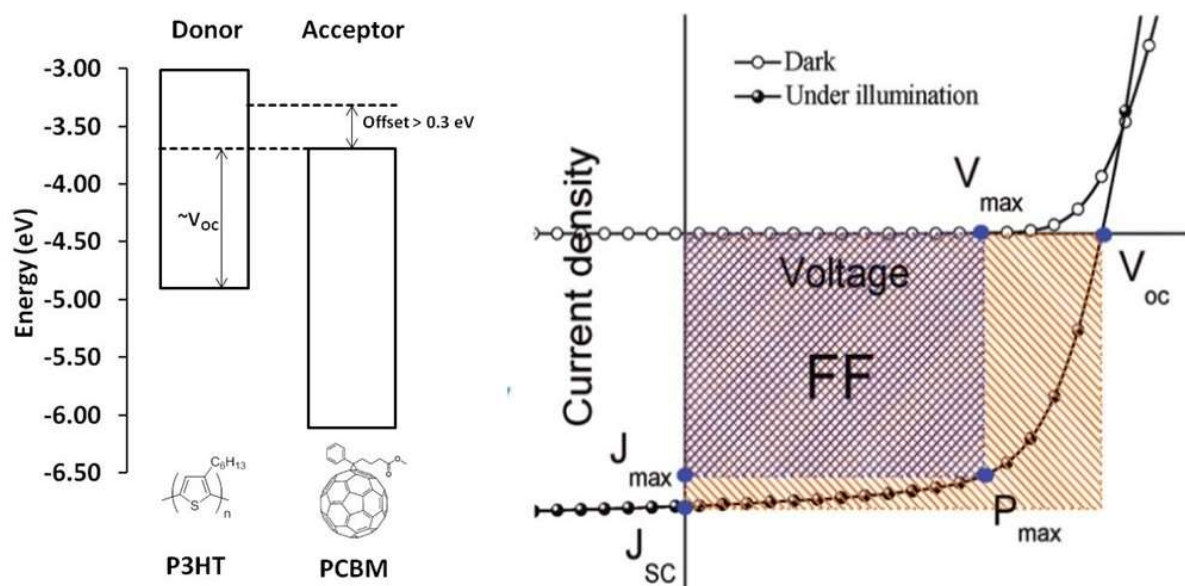

Figure 3. Energy level requirements and typical Current (J)-Voltage (V) characteristics of an OPV device.

Consequently, the four most important criteria that must be met by a donor polymer in an organic BHJ solar cell are as follows;

> ➢ A narrow electronic band-gap to absorb as much of the solar flux as possible.

> An appropriate level of crystallinity and fullerene miscibility to allow for formation of an ideal bicontinuous BHJ morphology.

> Appropriately placed frontier molecular orbital energy levels so as to ensure the maximum possible operating voltage of the solar cell whilst maintaining sufficient energetic offset with the acceptor to allow for efficient charge separation.

> A charge carrier mobility that is similar to that of the electron acceptor to ensure efficient and balanced charge extraction.

Through systematic chemical modifications, the performance of OPV cells has advanced impressively over the last three years, with PCE now routinely surpassing 10%.[7-9] Similar progress has been made with regards to charge carrier mobilities in OFETs, where OSC are currently achieving charge carrier mobilities exceeding those of amorphous silicon (~ 1 $cm^2.V^{-1}.s^{-1}$).[10, 11]

The most commonly studied polymeric materials are based on electron-rich aromatic moieties, such as thiophene, selenophene, fluorene, pyrrole, carbazole, and thieno[3,4-*b*]pyrazine (Figure 4), which have been reviewed at numerous occasions.[12, 13] A particularly interesting building block for the development of high performing polymeric semiconductors, however has received considerably less attention in current literature, 1,3-thiazole.
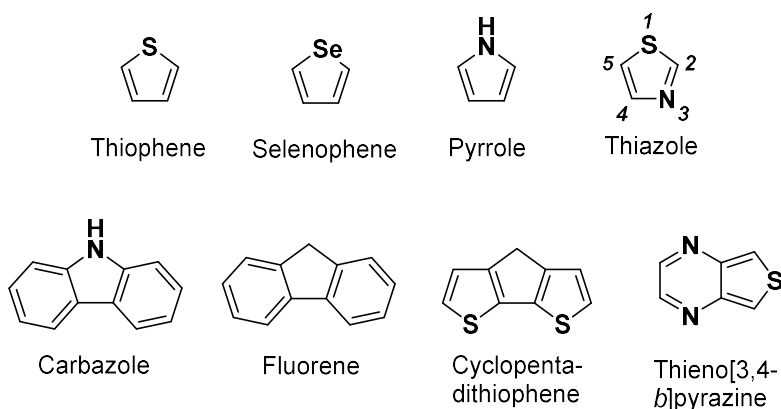

Figure 4: Chemical structures of several common aromatic building blocks encountered in conjugated polymers.

A common strategy to lower the frontier energy levels of conjugated materials is to incorporate electron-withdrawing elements or functional groups (*i.e.* F, CN, CF_3, …) into the polymer backbone. This approach however can be synthetically demanding and time-consuming, often relying on hazardous fluorinating or highly toxic cyanide reagents. An alternative and elegant

approach to lower both HOMO and the LUMO energy levels of π-conjugated compounds is to substitute a sp^2 carbon with a sp^2 nitrogen.[14-18] In contrast to the electron rich thiophene moiety, the isostructural thiazole unit is electron deficient due to the presence of the electronegative nitrogen in the five-membered ring. Besides the electronic effects introduced by the imine nitrogen in the thiazole ring, there are also regiochemical effects that need to be taken into account when incorporating 1,3-thiazole into conjugated polymers.

Due to the vast library of thiazole containing conjugated materials synthesized over the years, our focus in this review will be on π-conjugated small molecules and polymers containing bithiazole and fused bithiazole building blocks. Highlighting some of the most significant developments from 1999 to the present period (2016) reported in this field. The synthesis of well-defined oligomers and polymers of π-conjugated molecules based on thiazole unit is a considerable synthetic challenge that many groups have addressed over the last decade or so. This review is structured as follows; firstly we will briefly discuss the structural features of thiazole containing compounds, before discussing their physical properties. Our aim secondly is to summarize and discuss with several representative examples the wide range of bithiazole based molecules and polymers, in order to give the reader a comprehensive overview of the device performances of bithiazole containing compounds in OPV and OFET devices. Finally, we will discuss some newly designed acceptor building blocks that have the potential to be polymerized with fused bithiazole moiety, in order to obtain high performance acceptor polymers for use in bulk heterojunction solar cells and as organic field effect transistors. In order to validate our approach, we took advantage of density functional theory (DFT) calculations to predict geometric, electronic and optical properties of the five potential acceptors moieties presented.

Chemical and physical properties of bithiazoles

Although thiazole is often considered an electron-deficient version of thiophene, its reactivity is very different from thiophene and has to be considered when synthesizing thiazole based monomers. Due to the asymmetric nature of the thiazole ring, the π-electron density is highest on the C5 and lowest on the C2 carbon, which is also reflected in the reactivity of the thiazole moiety. Whereas nucleophilic aromatic substitution (S$_N$Ar) occur readily at the 2-position, electrophilic aromatic substitution (S$_E$Ar) take place preferentially at the 5- and 4-positions, making for example

the preparation of 2,5-dibrominated thiazole, a useful monomer for conjugated polymers, a rather tedious endeavor. In addition to the more complex reactivity, thiazole containing building blocks also present a more versatile regiochemistry, due to the C_s symmetry of the thiazole ring.

Coupling two thiazole rings, could theoretically yield six different bithiazoles (bTz), 2,2'-, 2,4'-, 2,5'-, 4, 4'-, 4,5'- and 5,5'-bithiazole, respectively. However, only three of those isomers are commonly used as building blocks in organic semiconductors and named according to their coupling position on the thiazole rings, head-to-head (HH- or 2,2'-bTz), head-to-tail (HT- or 2,5'-bTz), and tail-to-tail (TT- or 5,5'-bTz). As a consequence of the different geometries, different electronic and morphological effects have to be considered. Of the three isomers, the HT-bTz presents the largest overall dipole moment, whilst HH- and TT-bTz derivatives only possess local dipole moments due to the higher symmetry (Figure 5).
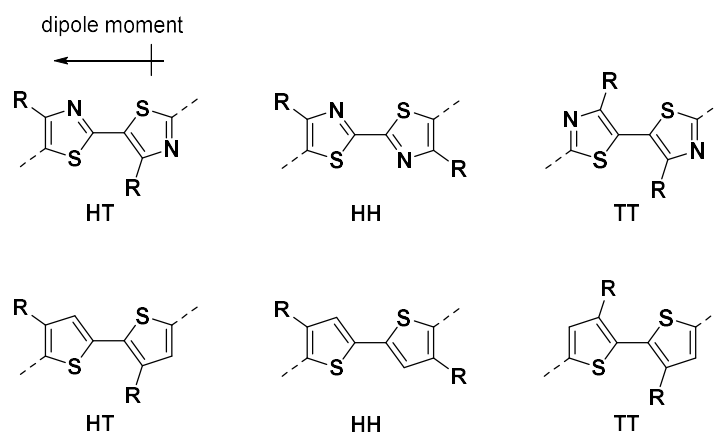

Figure 5: Chemical structures of head-to-tail (HT), head-to-head (HH) and tail-to-tail (TT) coupled bithiazole (top) and bithiophene (bottom) derivatives, R = alkyl chain.

The structural differences in regiochemistry are most pronounced when the thiazole rings bear substituents like bulky alkyl chains at the 4-position. HH-bTz and HT-bTz isomers present the smallest dihedral angles (<1°) between the two thiazole rings, whereas density functional theory calculations at the B3LYP/6-31G* level of approximation predict the largest dihedral angle (~70°) for the TT moiety.[19] The observed trend follows the observations previously made for alkylated bithiophene derivatives, however there are significant differences between the absolute values. Whereas the HH-bTz and HT-bTz moieties are planar, the dihedral angles found in HH-, respectively HT-bithiophene, are significantly larger (~20° and ~30°).[19] The differences in dihedral

angles between the aforementioned bithiazole and bithiophene units can be explained by having a closer look at the structural and electronic properties of the thiazole and thiophene rings. First of all, the steric effects in both systems have to be considered. In contrast to 2,2'-bithiophene, the nitrogen atoms in the bTz moiety are not bearing any sterically hindering hydrogen atoms (in contrast to the C3 and C3' in the bithiophene), thus reducing the steric constraints by eliminating repulsive C-H---H-C interactions and facilitating the planarization of the HH-bTz unit.[20-22]
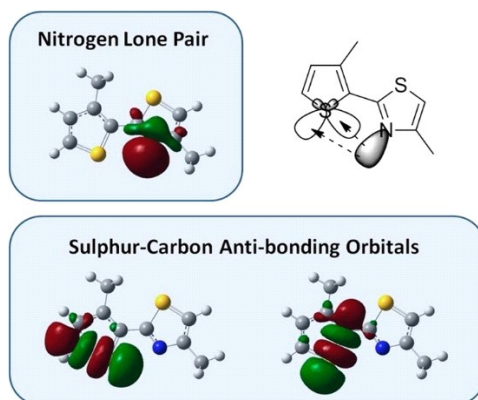

Figure 6: Visualization of nitrogen lone pair and carbon-sulfur antibonding orbitals. Reprinted with permission from *Chem. Mater.* **2013**, *25*, 4239-4249. Copyright 2016 American Chemical Society.[17]

In addition to the steric constraints, the electronic properties of thiazole have to be considered in order to fully explain the significant reduction in calculated dihedral angles between the HT-bithiophene (~30°) and HT-bithiazole (~0°). Bronstein *et al.* suggested a "conformational lock" mechanism in which the nitrogen lone pair of the thiazole ring interacts with the antibonding orbitals in the adjacent ring (Figure 6), thus favoring the planarization of the ring system.[23] Because such favorable interactions are absent in 2,2'-bithiophene, the geometry of the molecule is mainly dominated by the steric hindrance, thus yielding larger dihedral angles than HH- and HT-bTz units.

Bithiazole Based Small Molecules

Efforts to synthesize potential n-type materials have so far been limited. However, thiazole-containing conjugated small molecules/oligomers represent an attractive and promising class of materials, based on the idea that they can be used as functional elements and building blocks in the studies of molecular electronics. The optical properties and mobilities data for conjugated small

molecules/oligomers (**M1-M28**) are summarized in Table 1, and there corresponding structures are depicted in Figures 7, 8 and 15.

In 1999, Katz and co-workers reported the first bithiazole-based functionalized oligothiophene based semiconductor for OFETs.[24] Several p-type thiazole containing oligomers were synthesized with lower electron-donating ability than the parent sexithiophene. OFET device fabrication based on a dihexylated six membered ring compound with a bithiazole **M1** core showed hole mobility (μ_h) of 1.1×10^{-2} cm^2.V^{-1}.s^{-1}. Since then, several organic molecules containing bithiazole were synthesized as active materials for OFETs.

In 2003, Curtis and co-workers reported the synthesis of several co-oligomers based on 4,4'-dialkyl-2,2'-bithiazole and 3,4-ethylenedioxythiophene (EDOT) as donor-acceptor material.[25] They used the combination of having the bithiazole ring acting as a low energy LUMO acceptor with EDOT as the high energy HOMO donor to afford oligomers with lowered energy band gaps. Furthermore, the acceptor units of **M2** induce the co-oligomers to form π-stacked crystal structures with shorter intermolecular contact distances and effective interchain π−π orbital overlaps. However, no results on the fabrication and characterization of OFETs were reported until 2008, when the authors fabricated transistor having small and poorly connected crystallites using both vacuum deposition and solution casting for the butyl co-oligomer **M2**. The crystals were grown from bromobenzene solution that showed a hole mobility of 4×10^{-3} cm^2.V^{-1}.s^{-1}.[26]

In 2004, Yamashita and co-workers reported the novel synthesis of bithiazole-thiazolothiazole **M3** co-oligomers as n-type semiconducting active materials.[27] However, no OFET characteristics were observed in the films of **M3**, which the authors attributed to an improper molecular geometry in the thin film. Moreover, replacing thiazole with furan **M4** afforded good p-type semiconducting behavior and a mobility of 1×10^{-3} cm^2.V^{-1}.s^{-1}. The following year Yamashita and co-workers systematically prepared and investigated a series of bithiazole oligomers **M5-M7** and thiazole/thiophene **M8-M10** co-oligomers linked to trifluoromethylphenyl groups.[28] It was shown that by increasing the number of thiazole rings in the chain the electron affinity increased, this was attributed to the electron withdrawing properties of the thiazole ring. Interestingly, 2,2'-bithiazole **M6** had a higher electron affinity than that of 5,5-bithiazole **M5** despite having similar molecular structures and torsion angles (0° between the thiazole rings). Analyses of their X-ray crystal structures revealed a completely planar geometry for 5,5'-bithiazole **M5**, forming a unique 2-D

columnar structure. One of the molecules is bridged by two other units having an intermolecular separation of 3.37 Å between the stacked molecules, thus exhibiting good n-type performance with an electron mobility of up to 1.83 $cm^2.V^{-1}.s^{-1}$ on *n*-octadecyltrichlorosilane (OTS) treated substrates. In comparison, 2,2-bithiazole **M6** has a columnar structure with two crystallographically independent molecules having torsion angles of 1.6° and 10.4° between the 4-trifluoromethylphenyl and the thiazole units. **M6** did not show any OFET characteristics, indicating that the structure is not suited for high performance OFETs.[28]

Lee and co-workers in 2012, explored the possibility to use thiazole containing small molecules as active material in thin film devices. **M11** and **M12** were synthesized via stepwise Pd-catalyzed Suzuki and Stille coupling reactions.[29] The π-conjugated organic small molecule **M11** contains a rigid fused naphtha dithiophene core flanked by a bithiazole, whereas **M12** contains a triphenylamine-capped thiophene(3-decanyl)- bridged bithiazole. **M11** and **M12** exhibited similar absorption bands in the range of 300-540 nm and 300-550 nm, respectively. **M12** demonstrated an band gap (E_g) of 2.02 eV and a hole mobility of 2×10^{-6} $cm^2.V^{-1}.s^{-1}$. However, **M11** exhibited an E_g of 1.99 eV and a hole mobility of 1.5×10^{-5} $cm^2.V^{-1}.s^{-1}$. The higher mobility of **M11** was attributed to the co-planarity of the main chain and efficient intermolecular π-π stacking. The photovoltaic performance of the small molecules was evaluated by fabricating bulk heterojunction solar cells. The device with ITO/PEDOT:PSS/ **M11** and **M12**:PC$_{71}$BM/LiF/Al achieved a PCE of 1.09% with J_{sc} of 3.35 $mA.cm^{-2}$, V_{oc} of 0.80 V, and *FF* of 0.41 for **M11** and 1.62% with an enhanced J_{sc} of 4.47 $mA.cm^{-2}$, V_{oc} of 0.76 V, and *FF* of 0.48 for **M12**, respectively. It is worthy to note that **M12** has a lower V_{oc} than **M11** despite their similar HOMO levels. The authors attributed the reduced V_{oc} to the lower charge carrier mobilities caused by the charge recombination losses at the **M12**–PC$_{71}$BM interface and the electrodes.

Lin *et al.* reported the synthesis of a series of donor-acceptor-donor (D-A-D) small molecules **M13-M15** by Pd-catalyzed Suzuki or Stille coupling reactions, composed of the bithiazole-based acceptor, triphenylamine and thiophene as the donor units.[30] The small molecules showed an absorption maximum in film in the range of 406 to 498 nm, and an optical band gap ranging from 2.0 to 2.6 eV. Solution-processed OPVs based on **M15** exhibited the highest PCEs of 2.61% and a hole mobility of 3.6×10^{-4} $cm^2.V^{-1}.s^{-1}$. The extended π-conjugated length and electron

delocalization in compound **M15** improved the intermolecular interaction in the film, and thus, promoted good charge transport.[30]
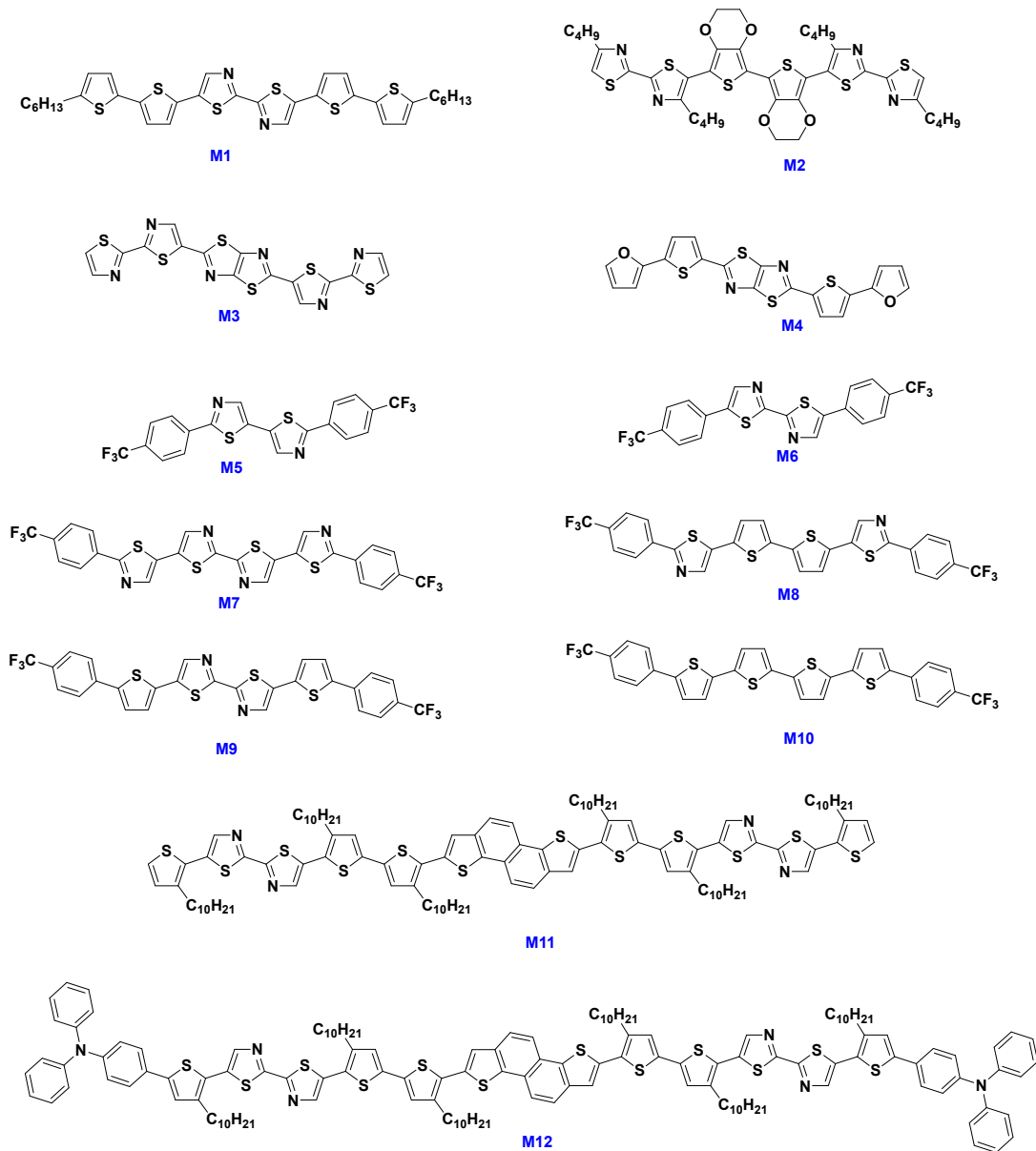

Figure 7: Chemical structure of bithiazole **M1-M9, M11-M12** and bithiophene based small molecule **M10**.

The fluorination of organic semiconductors is a popular approach to not only increase the stability towards atmospheric moisture, but also to introduce dipole moments into the semiconductors,

facilitating the self-assembly.[31-33] In 2014, Usta *et al.* reported the synthesis of perfluoroalkyl-functionalized thiazole-thiophene oligomers **M16**, **M17**, **M18** and **M19**.[34] OFETs with top-contact/bottom-gate device structures were fabricated from oligomers **M16-M19** by vacuum deposition. The devices exhibited n-channel behavior with high electron mobilities ranging from 0.20-1.30 $cm^2.V^{-1}.s^{-1}$. **M17**-based OFETs exhibited the highest electron mobility of 1.30 $cm^2.V^{-1}.s^{-1}$, an I_{on}/I_{off} of 10^6-10^7 and a threshold voltage (V_{th}) of +55 V at room temperature. The electron mobility was 4-5 times higher than the one reported for the thiophene counterpart having μ_e of 0.25 $cm^2.V^{-1}.s^{-1}$, I_{on}/I_{off} of 10^5-10^6 and V_{th} of +53 V. Interestingly, an increase of mobility was observed by increasing the deposition temperatures from 25 to 70°C for the larger oligomers **M18** (0.30 $cm^2.V^{-1}.s^{-1}$ → 0.70 $cm^2.V^{-1}.s^{-1}$) and **M19** (0.20 $cm^2.V^{-1}.s^{-1}$ → 0.50 $cm^2.V^{-1}.s^{-1}$). The improved device performance was attributed to better molecular arrangement and packing of the larger oligomers.

Jin and co-workers most recently, reported the synthesis of two biphenyl end-capped bithiazole co-oligomers, **M20** and **M21** for OFET.[17] **M20** and **M21** showed wide optical band gaps of 2.81 eV and 2.92 eV, respectively. The bottom-gate/top-contact OFETs were fabricated via vacuum deposition of **M20** with a 2,2'-bithiazole central unit exhibits a higher hole mobility of 3.5 $cm^2.V^{-1}.s^{-1}$ with I_{on}/I_{off} ratio of 10^8 and a V_{th} of -28 V. **M21** however showed a lower hole mobility of 0.4 $cm^2.V^{-1}.s^{-1}$ and I_{on}/I_{off} 10^5. The thin films of **M21** was found to have rough surface morphology and obvious grain boundaries, as a result higher potential barriers between the grains and lower charge transfer efficiencies were observed.
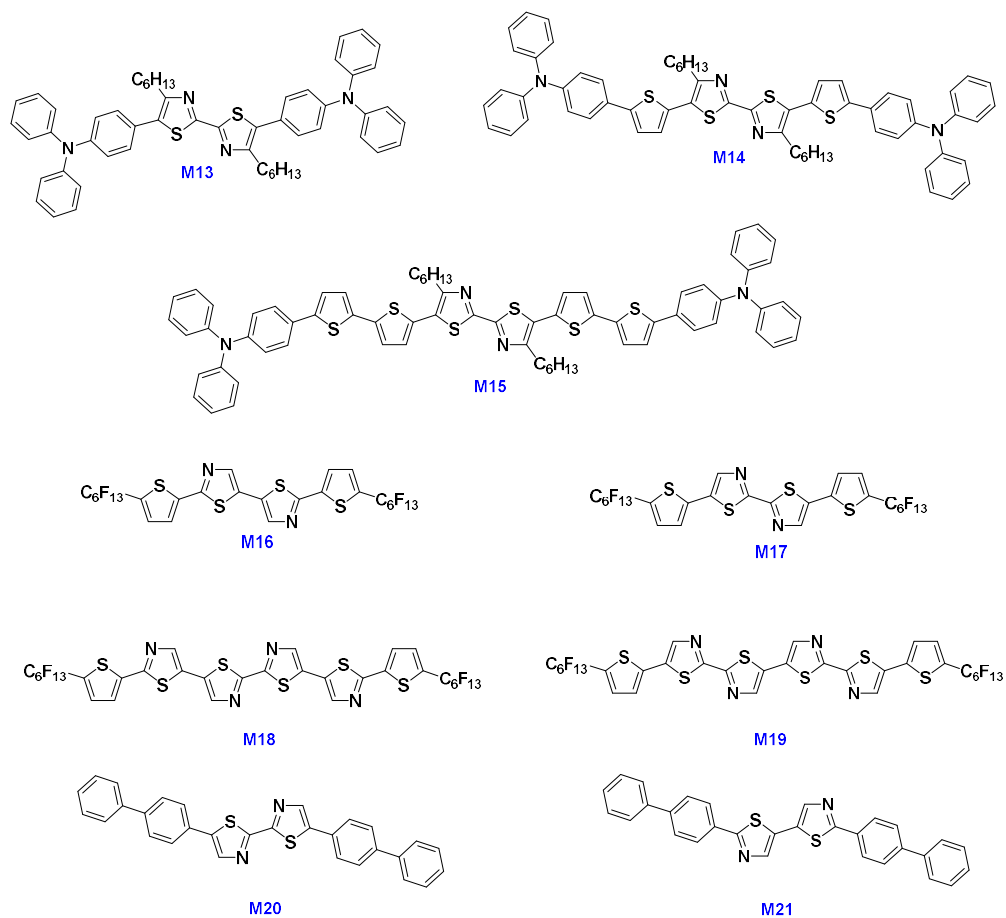
Figure 8: Chemical structures of bithiazole based small molecules **M13**-**M21.**

Table 1. Summary of optical band gap and thin-film OFET device data for bithiazole based small molecules **M1-M28**

	E_g^{opt} [eV]	Max μ_h [cm^2.V^{-1}.s^{-1}]	Ref.
M1	-	1.1×10^{-2}	24
M2	-	4×10^{-3}	25, 26
M4	-	1×10^{-3}	27
M5	2.90	1.83 [a]	28
M7	2.57	2.8×10^{-3}	28
M8	2.44	8.5×10^{-2}	28
M9	2.42	1.8×10^{-2}	28
M10	2.45	2.5×10^{-2}	28
M11	1.99	1.5×10^{-5}	29
M12	2.02	2×10^{-6}	29
M14	2.21	6.5×10^{-5}	30
M15	2.03	3.6×10^{-4}	30
M16	2.78	0.30 [a]	31
M17	2.77	1.30 [a]	31
M18	2.35	0.70 [a]	31
M19	2.35	0.50 [a]	31
M20	2.81	3.50	17
M21	2.92	0.40	17
M27	-	6×10^{-2} [a]	77
M28	-	2×10^{-3} [a]	77

[a] electron mobility μ_e

Bithiazole Based Polymers

The fused configuration of fluorene has brought many advantages in the area of conductive polymers, including coplanar geometry, good π-conjugating structure, and stable redox electrochemistry. Such advantages resulted in the first successfully developed blue-light-emitting materials.[35, 36] Jung and co-workers in 2005 were the first to report the synthesis of alternating conjugated polymers **P1** and **P2** based on alkylated 2,2-bithiazole and fluorene units via palladium-catalyzed Suzuki polymerization. Organic solar-cell devices having the structure ITO/PEDOT:PSS/PC$_{60}$BM:**P2** /Ca/Al showed very low PCE of 0.52%.[37] In 2008, Shim and co-authors reported the synthesis of **P3** by shifting the alkyl chain from the thiazole ring in **P2** to the thipohene unit. Light-emitting devices with ITO/PEDOT:PSS/**P3**/biBAlq/LiF/Al configurations were fabricated which resulted in a maximum brightness of 1750 cd.m^{-2}, maximum current efficiency of 0.91 cd.A^{-1}, and a maximum external quantum efficiency of 0.5%.[38]

Due to reduced rotational disorder along the polymer backbone, cyclopentadithiophene (CPDT)-based polymers possess longer π-conjugation lengths than polythiophene or polyfluorene derivatives and as a result better packing in solid state, which in turn improves the charge transport characteristics.[39-41] In 2009, Lin and co-workers introduced the coplanar CPDT unit into polymers **P1** and **P2** instead of the fluorene units as a structural modification. Interestingly, bulk heterojunction solar cells based on the newly synthesized copolymers **P4** and **P5** blended with [6,6]-phenyl C61 butyric acid methyl ester (PC$_{61}$BM) displayed significantly higher PCEs of 2.45 and 3.04%. Moreover, powder X-ray diffraction (XRD) analyses revealed a highly self-assembled π-π stacking structure in the solid state.[42] In 2010, improved PCEs of 3.55 and 3.80%, respectively, were reported by Chu and co-workers using the same low bandgap bithiazole based polymer **P5**, but changing the fullerene derivatives (PC$_{71}$BM or bisPC$_{61}$BM).[43] The enhanced PCEs were mainly attributed to the higher LUMO energy level of bisPC$_{61}$BM and the large increase in absorbance of PC$_{71}$BM relative to those of PC$_{61}$BM. The same year Lin and co-workers introduced 2,7-carbazole as the electron donor affording polymers **P6-P9**. The carbazole-based polymers **P6-P9** showed low HOMO levels, and high V_{oc}'s.[44] BHJ OPV devices were fabricated using polymers **P6-P9** and PC$_{61}$BM or PC$_{71}$BM in different weight ratios. A blend of 1:1.5 w/w (**P9**:PC$_{71}$BM) showed the best PCE of only1.01% with a J_{sc} of 4.83 mA.cm^{-2}, a V_{oc} of 0.60 V, and a FF of 0.35. Replacing the donor units of carbazole **P10** and dithienopyrrole **P11** with dithienosilole **P12** afforded higher PCE values based on **P12**:PC$_{70}$BM = 1:1(w/w) of 2.86% with J_{sc} of 7.85 mA.cm^{-2}, V_{oc} of 0.68 V, and FF of 0.54.[45] Chu and co-workers in 2011 improved the power conversion efficiency of polymer **P12** to 3.33% with J_{sc} of 8.7 mA.cm^{-2}, V_{oc} of 0.73 V, and FF of 0.52 by increasing the molecular weight (M_w) of the polymer.[46] Moreover, morphological analysis indicated that an increase in the M_w enhances polymer chain aggregation and interconnectivity within the bi-continuous network, which in return enhanced the charge transport properties by creating continuous percolation pathways. In the same year Li and co-workers reported the synthesis of polymer **P13** prepared via Pd-catalyzed Stille-coupling reaction, by incorporating longer alkyl chains (C$_9$H$_{13}$) on the thiazole unit and introducing a C$_6$H$_{13}$ group on the thiophene unit. The polymer exhibited lower HOMO energy level of -5.07 eV and PCE of 4.46% with J_{sc} of 9.01 mA.cm^{-2}, V_{oc} of 0.82 V, and FF of 0.60 under the illumination of AM1.5, 100 mW.cm^{-2}.[47]

By using longer *n*-nonyl side chains on the bithiazole (**P14** and **P15**), Zheng et al. were able to enhance the solubilty of **P12**.[48] Although both polymers showed similar band gaps, polymer **P14**

with a thiophene bridge showed a hole mobility of 1.46×10^{-4} cm^2.V^{-1}.s^{-1}, which is an order of magnitude higher than that of **P15** (1.25×10^{-5} cm^2.V^{-1}.s^{-1}), owing to the high molecular weight and enhanced backbone planarity of the polymer. The optimized **P14** device ITO/PEDOT:PSS/**P14**:PC$_{71}$BM/Al demonstrated a PCE of 3.46% with J_{sc} of 9.39 mA.cm^{-2}, V_{oc} of 0.65 V, and *FF* of 0.57, on the other hand, **P15** without the bridged thiophene exhibited lower PCE of 2.00 % with J_{sc} of 5.70 mA.cm^{-2}, V_{oc} of 0.86 V, and *FF* of 0.41. The high efficiency for polymer **P14** is owed to the higher hole mobility and better crystallinity. Moreover, the PCE of **P14** (3.46 %) was slightly higher than that of **P12** (3.33%),[46] which can be attributed to the high molecular weight and good solubility.

Shim and co-workers substituted the bridging silicon in the polymers, to afford CPDT based bithiazole copolymers. The CPDT unit was substituted with two different side chains, the branched 2-ethylhexyl **P16** and linear octyl groups **P17**.[49] The octyl-containing polymer **P17** showed relatively poor solubility and partial aggregation in solution due to the less sterically hindering linear side chains. Both **P16** and **P17** showed relatively poor OFET performances with maximum hole mobilities of 2.0×10^{-6} cm^2.V^{-1}.s^{-1}. In the case were the polymers blended with PC$_{61}$BM, the OPV device performance varied and **P16** exhibited a PCE of 1.12% with J_{sc} of 4.83 mA.cm^{-2}, V_{oc} of 0.69 V, and *FF* of 0.33. This was higher than achieved with **P17** (PCE = 0.59%, J_{sc} = 2.54 mA.cm^{-2}, V_{oc} = 0.68 V, *FF* = 0.34). The differences in device performance were attributed to the better solubility of **P16** and the higher miscibility of the fullerene derivative in the polymer phase.
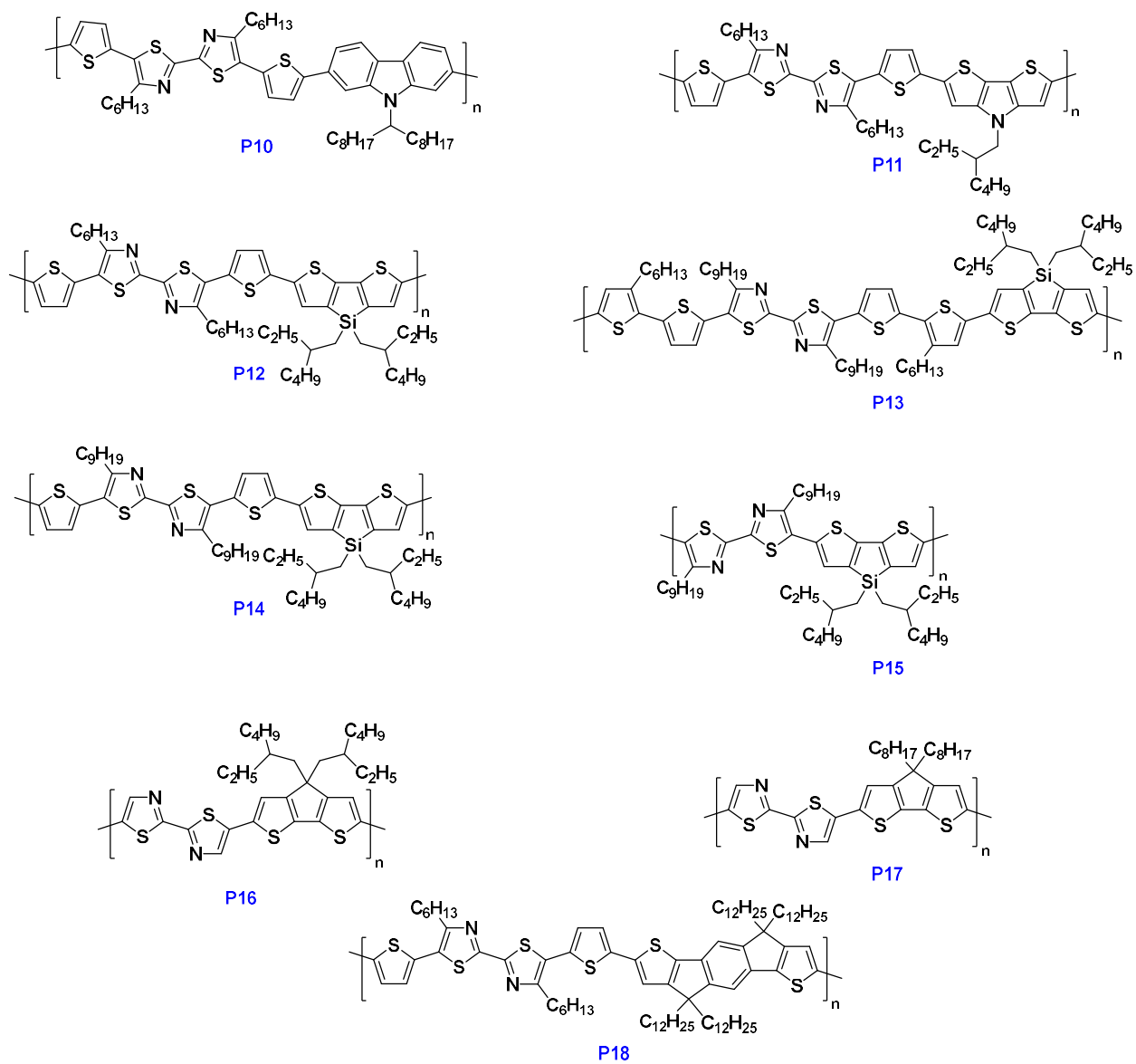
P1

P2

P3

P4

P5

P6

P7

P8

P9
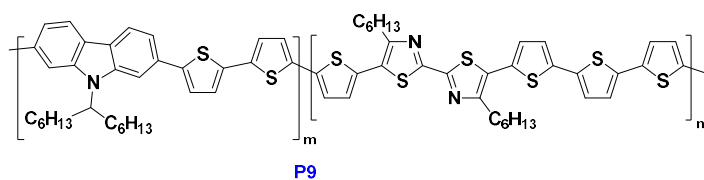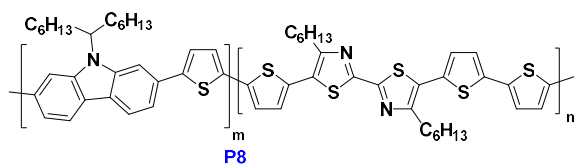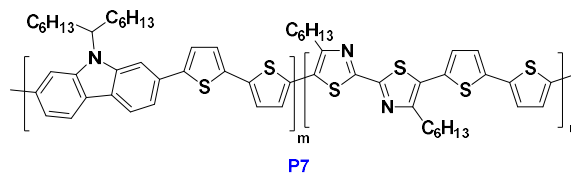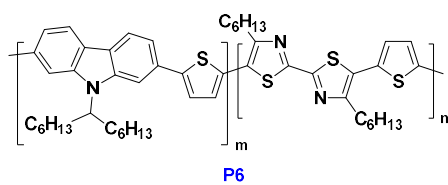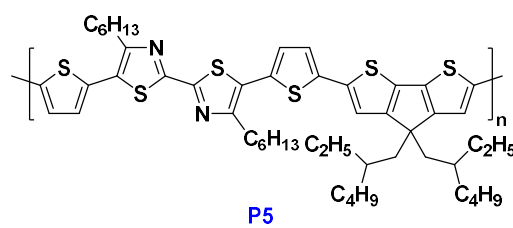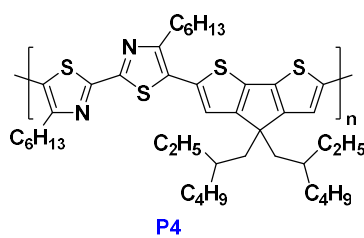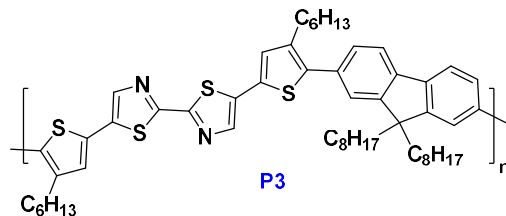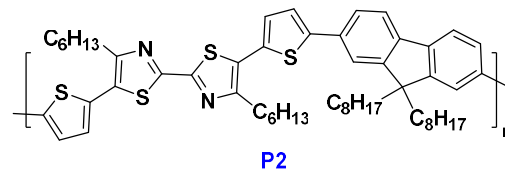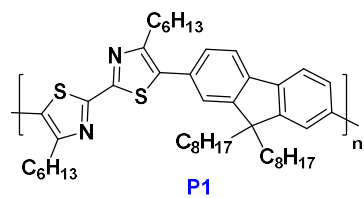
Figure 9- Chemical structure of bithiazole polymers **P1-P18**.

Table 2. Summary of the optoelectronic properties, energy levels, mobilities and photovoltaic properties of the polymers **P1-P18**.

	M_n [kDa]	PDI	E_g^{opt} [eV]	HOMO/LUMO [eV]	Max μ_h [cm^2.V^{-1}.s^{-1}]	J_{sc} [mA.cm^{-2}]	V_{oc} [V]	FF	PCE [%]	Ref.
P1	18.4	2.47	2.60	-5.85/-2.67	-	-	-	-	-	34
P2	49.3	2.08	2.21	-5.53 /-2.77	-	1.70	0.76	0.40	0.52	34
P3	70.4	2.68	2.28	-5.70/-2.82	-	-	-	-	-	35
P4	15.1	1.34	1.94	-5.40/-3.57	5.4×10^{-4}	6.34	0.73	0.53	2.45	39
P5	17.7	1.81	1.84	-5.07/-3.33	2.5×10^{-3}	7.30	0.88	0.59	3.80	39,40
P6	41.9	1.62	1.99	-5.42/-3.60	-	1.93	0.53	0.35	0.36	41
P7	25.1	1.36	1.96	-5.40/-3.59	-	2.31	0.56	0.36	0.46	41
P8	8.9	1.20	1.98	-5.38/-3.58	-	2.52	0.62	0.37	0.57	41
P9	8.6	1.19	1.93	-5.34/-3.55	-	4.83	0.60	0.35	1.01	41
P10	73.7	3.40	2.21	-5.44/-2.91	1.0×10^{-6}	1.24	0.82	0.30	0.30	42
P11	4.6	1.78	1.68	-4.76/-2.79	5.0×10^{-5}	0.51	0.28	0.34	0.06	42
P12	5.6	1.70	1.85	-5.18/-3.09	3.1×10^{-4}	7.85	0.68	0.54	2.86	42
	33.6	1.15	-	-	1.9×10^{-5} 2.7×10^{-5} ^{a}	8.70	0.73	0.52	3.33	43
P13	9.1	1.61	1.89	-5.07/-2.92	-	9.01	0.82	0.60	4.46	44
P14	44.1	1.30	1.87	-5.12/-3.25	1.46×10^{-4}	9.39	0.65	0.57	3.46	45
P15	8.8	1.80	1.85	-5.35/-3.50	1.25×10^{-5}	5.70	0.86	0.41	2.00	45
P16	7.8	1.64	1.89	-5.20/-3.44	2.0×10^{-6}	4.83	0.69	0.33	1.12	46
P17	8.9	1.87	1.86	-5.24/-3.43	2.0×10^{-6}	2.54	0.68	0.34	0.59	46
P18	13.6	1.83	2.00	-5.26/-2.80	5.0×10^{-4}	7.43	0.90	0.41	2.77	48

^{a} electron mobility μ_e

The pentafused indacenodithiophene (IDT) donor unit has attracted significant interest in recent years. When incorporated into low bandgap donor-acceptor copolymers, the energetic disorder along the conjugated backbone can be dramatically minimized, allowing nearly disorder free charge transport along the polymer backbone.[50] Li and co-workers synthesized copolymer **P18** incorporating the acceptor bithiazole moiety via Pd-catalyzed Stille coupling.[51] Copolymer **P18** exhibited an absorption maximum at relatively short wavelengths in comparison to other acceptors such as bis(thiophen-2-yl)thiazolothiazole (TTz), bis(thiophen-2-yl)-tetrazine (TZ), and bis-(thiophen-2-yl)-benzothiadiazole (DTBT). The rather large bandgap was attributed to BTz being a rather weak acceptor unit, in addition to steric effects twisting in the polymer backbone due to the presence of the hexyl side chains on the thiazole unit. Solution-processed OFET devices based on polymer **P18** showed hole mobility of 5.0×10^{-4} cm^2.V^{-1}.s^{-1} and PCE of the polymer solar cell based on **P18**/PC$_{71}$BM (1:2 w/w) of 2.77% with J_{sc} of 7.43 mA.cm^{-2}, V_{oc} of 0.90 V, and FF of 0.41

under the illumination of AM1.5G, 100 mW.cm^{-2}. The low performance of the **P18** was attributed to unfavorable BHJ morphology as evidenced by atomic force microscopy (AFM) measurements. The polymer/ PC$_{71}$BM film showed extensive phase separation with a domain sizes exceeding 100 nm and large surface roughness (4-5 nm). Table 2 provides a summary of the optoelectronic properties, energy levels, mobilities and photovoltaic properties of the polymers **P2-P18** shown in Figure 9.

Wong et al. synthesized a series of conjugated metallopolymers offering broad solar absorptions and tunable solar cell efficiency based on platinum(II) polyynes containing bithiazole-oligo(thienyl) units. [52] The advantage of having different π conjugation bridge length, can result in tuning the charge transport and photovoltaic properties of these copolymers. OPV devices were fabricated using the polymer **P19** as electron donor and PC$_{61}$BM as the electron accepting material. The device performance varied and was dependent to a large extent on the number of thienyl rings along the main polymer chain. A considerable increase in the short circuit current density (J_{sc}) and PCE was observed for polymer **P19** (6.50 mA.cm^{-2} and 2.5%) having eight heterocycles in the repeat unit, in comparison to the polymer with two heterocyclic units with a J_{sc} of 0.91 mA.cm^{-2} and PCE of 0.21%. Moreover, it was reported that an increase in the number of thienyl rings in the chain would result in an increase of the intrachain mobility, due to the more extended π-conjugation. Thus, affording polymers that exhibit higher carrier mobilities.[52]

Lee et al. reported the synthesis of a new type of π-conjugated copolymers via polycondensation reaction using a nickel catalyst. [53] Copolymers **P20** and **P21** are composed of an electron-donating bithiophene and an electron-accepting 5,5'-bithiazole. The authors also investigated whether or not the planarity of the polymer backbone could be enhanced through the regiochemistry of the alkyl group side-chains. Due to the head-to-head linkages in copolymer **P20**, the steric hindrance between alkyl side chains along the polymer is significantly reduced, thus allowing the polymer to adopt a more ordered coplanar-backbone conformation. As a result of the improved backbone planarity, a large red shift from solution to the film state (92 nm) was observed for the UV-vis of **P20**. In contrast, **P21** showed a slightly smaller shift (76 nm), most likely because the polymer chains already partially aggregate in solution due to the lack of side chains on the backbone. Top-contact/bottom-gate OFETs were fabricated from chlorobenzene solution on pretreated SiO$_2$

substrates by spin coating. **P20** showed typical p-type behavior with a mobility of 0.001 $cm^2.V^{-1}.s^{-1}$, having a low off-state current of about 1 pA.[53]

The same group later introduced didodecyl side chains on both thiophene and thiazole to afford copolymer **P22**. As a result, the ionization potential (IP) was increased, due to the enhanced rotational freedom along the backbone and the electron-accepting nature of the 5,5'-bithiazole units. Copolymer **P22**-based OFETs exhibited electron mobilities as high as 0.33 $cm^2.V^{-1}.s^{-1}$ and unprecedented bias-stress stability comparable to that of amorphous silicon.[54] Li and co-workers in 2011, introduced three conjugated D-A copolymers **P23, P24**, and **P25**, containing the bithiazole acceptor with different alkyl chain lengths (hexyl, nonyl and undecyl).[55] The polymers exhibited broad absorption spectra ranging from 350 to 650 nm in thin films. Similar HOMO and LUMO energy levels were reported for all polymers. BHJ solar cells based on **P24** showed the highest PCE of 2.58% with V_{oc} of 0.77 V, a J_{SC} of 8.70 $mA.cm^{-2}$, and a FF of 0.39. **P25** based OPVs exhibited slightly lower performance (PCE =2.15%, V_{oc} = 0.81 V, J_{SC} = 5.91 $mA.cm^{-2}$, FF = 0.45), indicating that the length of the alkyl chains influences the photovoltaic properties of the polymers.[55] In 2012, the same authors introduced thieno[3,2-*b*]thiophene into polymer **P23** instead of thiophene as a structural modification. The newly synthesized crystalline D-A copolymer **P26** possessed high thermal stability (T_d = 450 °C) and a lower-lying HOMO energy level at -5.20 eV.[56] Ordered and densely packed side chains on the polymer resulted in hole mobilities of 6.45×10^{-3} $cm^2.V^{-1}.s^{-1}$. In OPV devices based on **P26**:$PC_{71}BM$ (1:1 w/w), PCE values of 4.57% (V_{oc} = 0.82 V, J_{SC} = 9.89 $mA.cm^{-2}$, FF = 0.56) were achieved. A higher PCE of 5.35% was achieved when the $PC_{71}BM$ acceptor was substituted with a new fullerene derivative, indene-C_{60} bisadduct (ICBA) having a LUMO energy level of -3.74 eV. Moreover, a higher V_{oc} of 1.03 V, a J_{SC} of 8.55 $mA.cm^{-2}$, and a FF of 0.61 were achieved.[56]

In 2009, solution processable donor–acceptor copolymers with *N*-alkyldithieno[3,2-*b*:2',3'-*d*]pyrroles (DTP) and bithiazole units, **P27-P28** were synthesized by McCullough and co-workers.[57] The relatively electron deficient and rigid bithiazole unit in comparison to bithiophene, in the DTP- in effect can lower the HOMO energy levels and afford more rigid, planar polymers. Their study revealed that high hole mobilities can be achieved without post-deposition thermal annealing. **P27-P28** achieved field effect mobilities of 4.2 x 10^{-2} and 0.14 $cm^2.V^{-1}.s^{-1}$ with current on/off ratios up to 10^6. Moreover, there was no significant degradation in air of the device over 60

days, demonstrating excellent air stability.[57] Such co-polymers based on the DTP-bithiazole provides yet another example where high performance does not require high crystalline ordered structures. Lin and co-workers in 2011, reported the synthesis via Suzuki coupling polymerization for a series of alternative D-A conjugated DTP-based polymers.[58] The DTP unit had the minimum-branched alkyl chain (ethyl-ethyl group) length and the electron-deficient bithiazole contained the liner alkyl chain (hexyl groups). The absorption maxima of polymers **P29–P33** were in the range of 480-522 nm and 508-558 nm for solution and the solid state films, respectively. However, polymer **P29** possessed the least red-shifted absorption maxima and polymer **P33** showed a blue-shift from solution to the solid film. This was attributed to the twisting of the polymer backbone as a result of the hexyl side-chains on the thiophene and bithiazole units. All the polymers showed poor hole and electron mobilities, in the ranges of 10^{-8} to 10^{-7} and 10^{-7} to 10^{-6} cm^2.V^{-1}.s^{-1}, which was attributed to the low molecular weight of the polymers. BHJ solar cells comprised of ITO/PEDOT:PSS/(**P29–P33**) were fabricated and showed V_{oc} values in the range of 0.18-0.62 V. Polymer **P30** achieved the highest V_{oc} value due to its lower HOMO level. Among all the polymers **P32** offered the best PCE of 0.69% under AM 1.5 (100 mW.cm^{-2}) illumination with a V_{OC} of 0.40 V, a J_{SC} of 4 mA.cm^{-2}, and a FF of 0.43.[58] Table 3 provides a summary of the optoelectronic properties, energy levels, mobilities and photovoltaic properties of the polymers **P19-P33** shown in Figure 10.

Two polymers, one containing a bithiophene unit **P34** and the other bithiazole **P35** were synthesized and reported by Paek *et al.* Even though the polymers have similar chemical structures, they exhibit very different electronic properties.[59] A highly ordered structure by XRD, reduced band-gap and lowered HOMO and LUMO levels were reported for polymer **P35**, when compared to **P34**. Bithiazole-containing polymer **P35** exhibited higher on/off ratio (4.7×10^4) and a higher mobility of 1.1×10^{-3} cm^2.V^{-1}.s^{-1} versus **P34** with lower on/off ratio (1.1×10^3) and a mobility of 6×10^{-5} cm^2.V^{-1}.s^{-1}.[59]
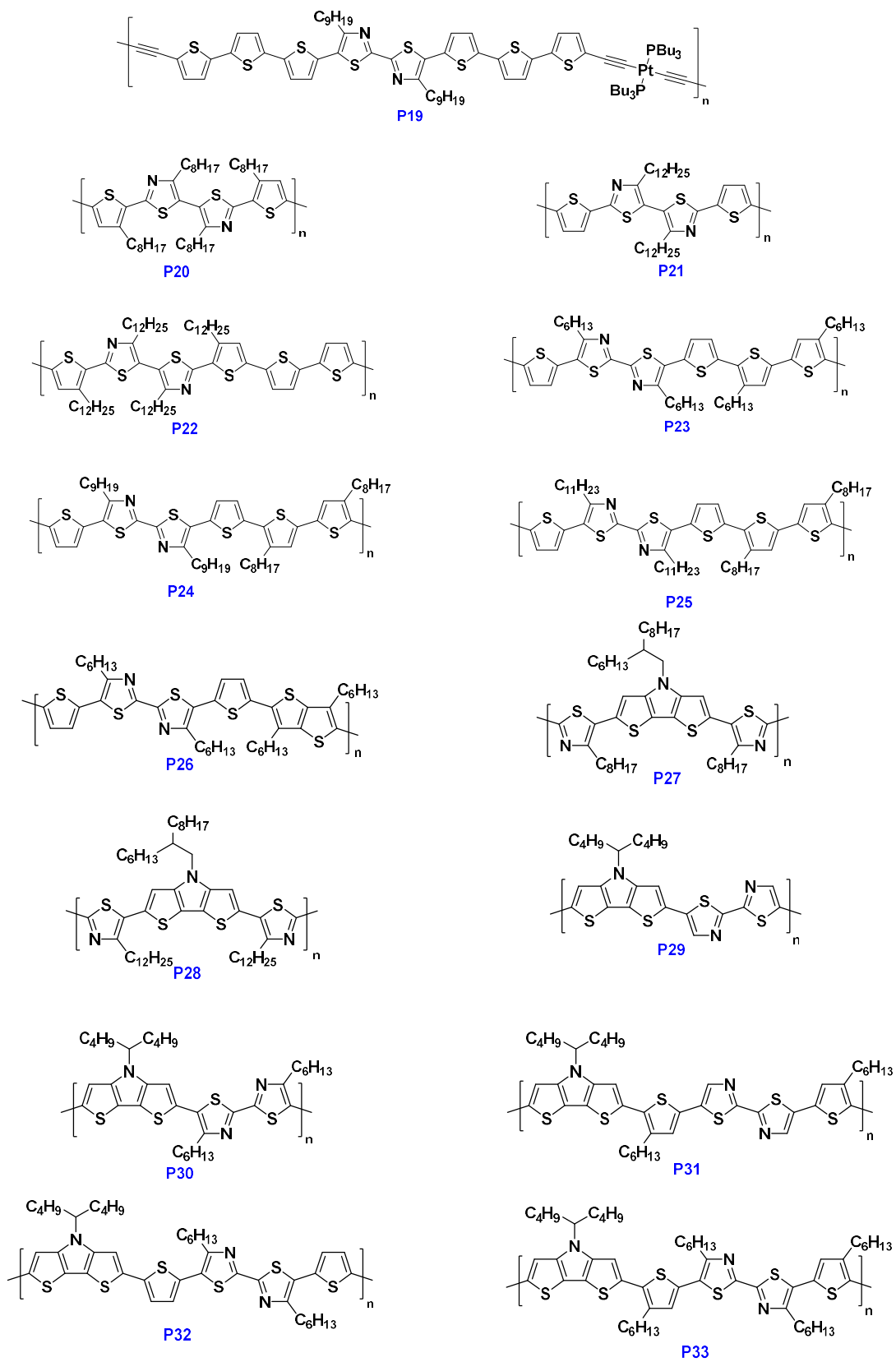
Figure 10- Chemical structure of bithiazole polymers **P19**-**P33**.

Table 3. Summary of the optoelectronic properties, energy levels, mobilities and photovoltaic properties of the polymers **P19-P33**.

	M_n [kDa]	PDI	E_g^{opt} [eV]	HOMO/LUMO [eV]	Max μ_h [cm^2.V^{-1}.s^{-1}]	J_{sc} [mA.cm^{-2}]	V_{oc} [V]	FF	PCE [%]	Ref.
P19	15.7	1.83	2.06	-5.71/-3.65	-	6.50	0.88	0.44	2.50	49
P20	45.0	2.40	-	-5.15/-	10^{-3}	-	-	-	-	50
P21	20.0	-	-	-5.20/-	10^{-6}	-	-	-	-	50
P22	13-41	1.4-1.7	-	-5.19/-	0.33 [a]	-	-	-	-	51
P23	3.2	1.59	1.89	-5.18/-2.93	1.3×10^{-4}	5.67	0.66	0.31	1.17	52
P24	4.7	1.51	1.90	-5.20/-2.95	1.1×10^{-3}	8.70	0.77	0.39	2.58	52
P25	6.3	1.55	1.89	-5.23/-2.98	6.8×10^{-4}	5.91	0.81	0.45	2.15	52
P26	4.2	1.60	2.20	-5.20/-2.90	6.45×10^{-3}	8.55	1.03	0.61	5.35	53
P27	9.0	2.00	1.75	-5.23/-3.48	4.2×10^{-2}	-	-	-	-	54
P28	10.5	2.00	1.67	-5.22/-3.55	0.14	-	-	-	-	54
P29	10.7	1.04	1.76	-5.28/-3.76	9.6×10^{-8} 3.0×10^{-6} [a]	1.10	0.18	0.34	0.06	55
P30	34.0	1.93	1.74	-5.17/-3.54	3.2×10^{-8} 1.2×10^{-6} [a]	1.50	0.62	0.29	0.27	55
P31	45.0	2.02	1.71	-4.99/-3.55	5.3×10^{-8} 9.6×10^{-7} [a]	2.80	0.53	0.32	0.47	55
P32	22.6	1.27	1.68	-4.81/-3.59	2.2×10^{-7} 1.2×10^{-6} [a]	4.00	0.40	0.43	0.69	55
P33	10.9	1.15	1.79	-5.06/-3.71	4.2×10^{-8} 8.3×10^{-6} [a]	2.50	0.41	0.35	0.36	55

[a] electron mobility μ_e

Owing to its large planar structure and small steric hindrance between adjacent molecules benzodithiophene (BDT) moiety has emerged as an attractive building block for conjugated polymers, and has attracted wide interest for applications in OPVs and OFETs displaying good hole mobilities. In 2010, Li and co-workers reported the copolymerization of benzodithiophene (BDT) with bithiazole via Stille coupling reaction. Devices with ITO/PEDOT:PSS/**P36**:PC$_{71}$BM/Al structure exhibited a PCE of 3.82% under AM 1.5 (100 mW.cm^{-2}) illumination with a V_{OC} of 0.86 V, a J_{SC} of 7.84 mA.cm^{-2}, and a FF of 0.57. The high V_{OC} is attributed to the HOMO energy level of **P36** which was found to be significantly deeper (-5.15 eV) than that (-4.76 eV)[60] of poly(3-hexylthiophene) P3HT.[61]

A year later Zhan, Li and co-workers shortened the alkyl chains on the thiazole unit in **P36** to a hexyl group and focused on the relationship between morphology and device performance by optimizing the blend composition and additive content.[62] The authors explored the effect of blend

composition by altering the donor/acceptor weight ratio, from 1:1, 1:2 and 1:3 with the addition of 1-2% 8-diiodooctane (DIO). The best result for the BHJ solar cell with optimized morphology afforded PCE of ~3.2%, which was lower than the previous reported efficiency (3.82%).

In 2013, Shen *et al.* introduced yet another modification by attaching a conjugated thienyl side chain onto the thiazole unit.[63] Copolymers, **P37** and **P38** showed deeper HOMO energy levels of -5.19 and -5.26 eV, respectively, as a result of the thienyl side chains attached on BTz, in comparison to other BDT–BTz-based copolymer that have a alkyl side chain on the bithiazoles (-5.15 eV).[29] BHJ solar cell devices for **P37** and **P38** with a configuration of ITO/PEDOT:PSS/polymer:PC$_{71}$BM/Ca/Al and 3% w/w DIO displayed PCEs of 3.71% (V_{OC} = 0.78 V, J_{SC} = 10.30 mA.cm^{-2}, FF = 0.46) and 2.92% (V_{OC} = 0.82 V, J_{SC} = 7.18 mA.cm^{-2}, FF = 0.50), respectively. The high J_{SC} value of **P37** relative to **P38** was attributed to the high absorption ability of **P37**. The PCE for **P37** (3.71%) achieved was slightly higher than that of **P36** (3.2%) reported previously, which can be attributed to the hexylthiophene side chains attached on the bithiazole unit.

In 2011, Zhan and co-workers also reported the copolymerization of BDT with four bisthienyl-bithiazole units having different side chains by Pd-catalyzed Stille coupling.[64] Polymer **P39** was poorly soluble due to the coplanar structure and the resulting strong inter-chain interactions. The *n*-dodecyl side chains on the BDT moiety were replaced with branched 2-decyltetradecyl side chains to afford **P40**. Introducing *n*-dodecyl side chains onto the thiophene resulted in polymers **P41** and **P42**. The ionization potential of **P41** was lower than that of **P39**, **P40**, and **P42**, because of increased torsional angles along the polymer backbone with the HOMO wavefunction primarily located on the benzodithiophene and adjacent thiophenes. On the other hand, the HOMO wavefunctions of **P39**, **P40**, and **P42** are delocalized over the entire polymer backbones. BHJ solar cells with the following device structure ITO/PEDOT:PSS/**P40** (**P41** or **P42**):PC$_{71}$BM (1:1, w/w)/Ca/Al were fabricated to afford PCEs of 1.14% (**P40**), 0.09% (**P41**), and 2.54% (**P42**), respectively. V_{OC} of **P40** and **P42** were higher (0.91 and 0.82 V) than for **P41** (0.76 V) due to the lower HOMO energy level, this was attributed to the low mobility and morphological defects of the active layer. In 2014, the same group reported the charge carrier mobility and phototransistor performance for polymers **P39-P42**.[65] All the devices showed p-type characteristics under ambient atmosphere and among all the polymers **P40** exhibited the highest mobility of 0.19 cm^2.V^{-1}.s^{-1},

owing to the large and planar conjugated structure promoting π-π stacking with a highly ordered lamellar structure benefiting charge transport. Moreover, long term stability of **P40** based OFETs was investigated for 50 days and no noticeable changes in the on/off current ratio and mobility could be detected. Despite its high PCE **P42** (2.54%), the highest mobility achieved for **P42** was 0.18 cm^2.V^{-1}.s^{-1}. **P40**, and **P42** exhibited the best photo-responsivities of R_{max} =120 and 132 A.W^{-1}, and the best photocurrent/dark current ratios (P_{max} =1.4×10^5 and 2×10^5), which is directly related to the excellent charge transport properties of the polymers.
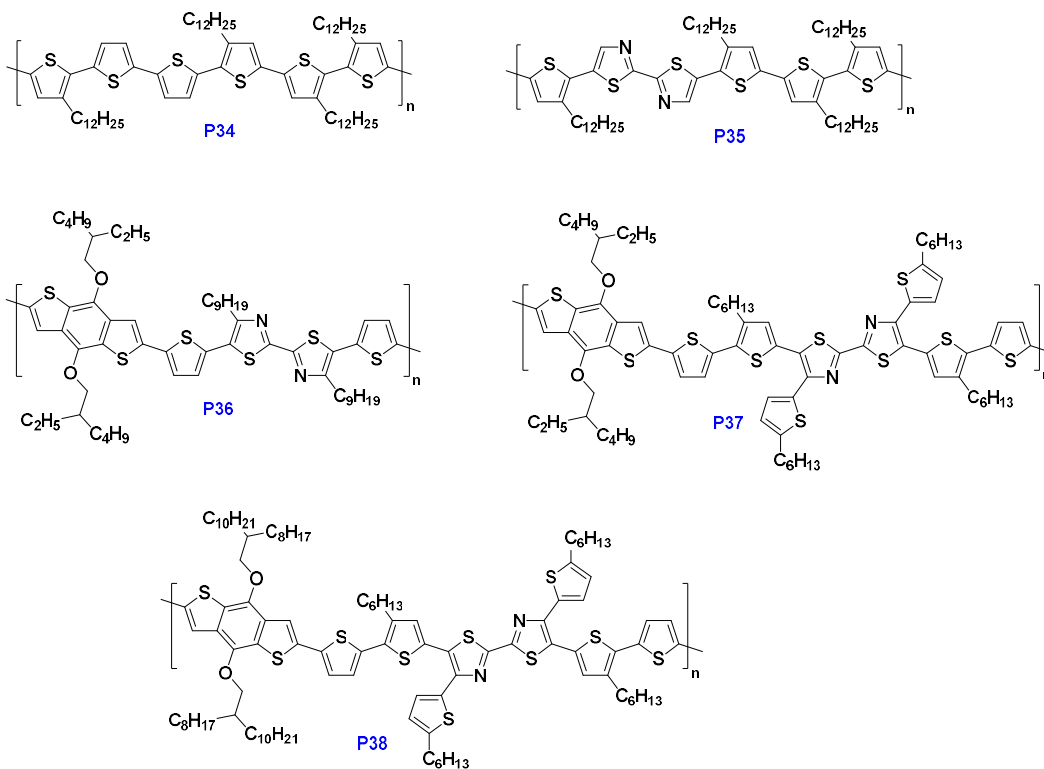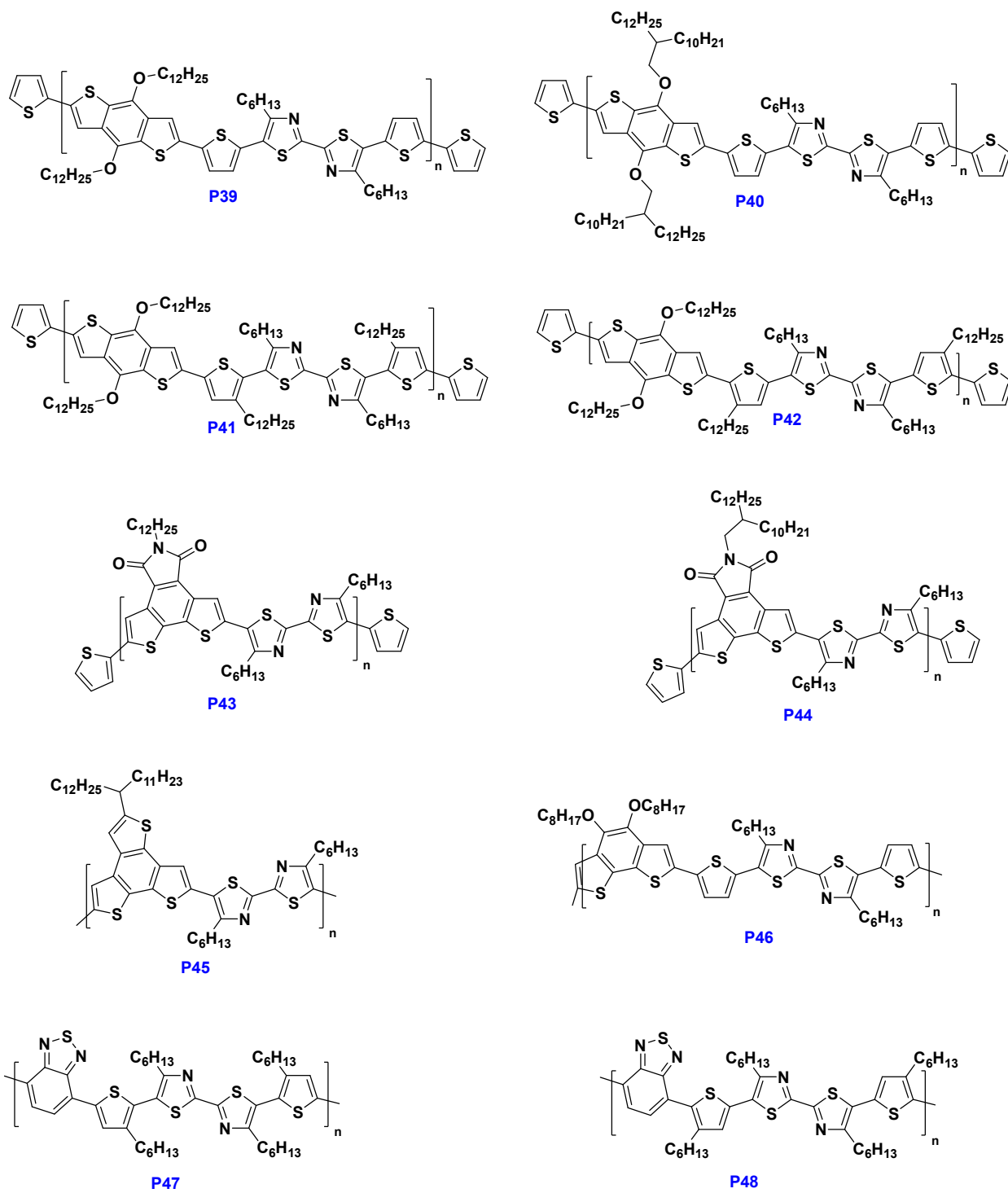
Figure 11- Chemical structure of bithiazole polymers **P34-P48**.

Zhan and co-workers also reported the synthesis of a series of conjugated copolymers based on dithienophthalimide coupled with bithiazole via Stille coupling to afford polymers **P43** and **P44**.[66] Polymer **P43** having three liner solubilizing *n*-alkyl groups had poor solubility as a result of the strong interchain interactions. Replacing *n*-dodecyl in **P43** with branched 2-decyltetradecyl unit significantly enhanced the solubility of **P44**. Both polymer **P43** and **P44** exhibited almost identical absorption profiles in solution and in thin films. The frontier energy levels (HOMO/LUMO) for both polymers were estimated to be -6.04/-3.04 eV (**P43**) and -6.02/-3.06 eV (**P44**). Unfortunately, the authors did not report any device performance for the polymers.

Yang and co-workers reported the synthesis of a planar conjugated polymer based on benzotrithiophene and bithiazole.[67] Copolymer **P45** has a deeper HOMO (-5.65 eV) energy level than that of P3HT and a band gap of 2.05 eV. The PCE of the pristine device BHJ solar cell fabricated under AM 1.5 (100 mW.cm^{-2}) illumination with the structure ITO/PEDOT:PSS/ **P45**:PCB$_{71}$M/LiF/Al illustrated a PCE of only 2.49% with a V_{oc} of 0.83 V, a J_{SC} of 6.22 mA.cm^{-2}, and a *FF* of 0.48. Treatment with 1 vol% DIO additive **P45** device displayed a higher PCE of 5.06% with a slightly lower V_{OC} (0.81) V, a higher J_{SC} (10.9 mA.cm^{-2}), and a *FF* of 0.57.

Copolymerization of dioctyloxybenzo[1,2-*b*:4,3-*b'*]dithiophene (BdT) unit with bithiazole has been prepared through Pd-catalyzed Stille-coupling to afford copolymer **P46** reported by Li and co-workers.[68] The polymer showed a broad absorption in the range of 300-650 nm and had an optical band gap of 2.01 eV. **P46** exhibited a relatively low HOMO energy level of -5.16 eV and a hole mobility of 5.53×10^{-4} cm^2.V^{-1}.s^{-1}. The BHJ solar cell fabricated with a configuration of ITO/PEDOT:PSS/ **P46**:PC$_{71}$BM/Ca/Al achieved a PCE of 2.81% with a V_{OC} of 0.88 V, a J_{SC} of 5.20 mA.cm^{-2}, and a *FF* of 0.61.

In 2012, Seki and co-workers reported the first example of an electron transporting (n-type) polymer **P47** and **P48** based on bithiazole unit for OPV.[69] **P47** was synthesized using Suzuki copolymerization between bithiazole and benzothiadiazoles, whereas Stille polycondensation was adopted for the synthesis of **P48**. The two polymers differ in their side chain positioning at the thiophene units sandwiching the bithiazole unit. The polymers showed a broad absorption in the range of 300-700 nm and had an optical band gap of 1.64 and 1.74 eV, respectively. Photoconductivity of polymers **P47** and **P48** in the film state were measured using flash-photolysis time-resolved microwave.

The intrinsic charge carrier mobilities of **P47** were found to be 2.1×10^{-4} cm^2.V^{-1}.s^{-1}. In the presence of an additive (1,8-octanedithiol) the carrier mobilities improved slightly to 6.5×10^{-4} cm^2.V^{-1}.s^{-1}. No measurable photoconductivity signals were obtained with polymer **P48**.

Following the successful synthesis of small molecules **M11** and **M12**, Lee and co-workers turned their attention to expanding the scope of their studies, by synthesizing the D-A conjugated copolymer **P49** via Stille cross-coupling reaction.[70] The resulting polymer showed a narrow absorption in the range of 350-650 nm and had an optical band gap of 1.98 eV. The **P49** copolymer exhibited typical p-type organic semiconductor characteristics with low hole mobility of 7.9×10^{-5} cm^2.V^{-1}.s^{-1}, which is attributed to the rather low molecular weight. BHJ solar cells with ITO/PEDOT:PSS/ **P49**:PC$_{71}$BM/LiF/Al configuration were fabricated with various blend ratios (1:1 to 1:4 w/w). The device performance varied in the range of 0.45%-0.76% based on the blend ratios. The highest PCE based on **P49**:PC$_{71}$BM (1:4 w/w) was 0.76% with a V_{OC} of 0.70 V, a J_{SC} of 3.15 mA.cm^{-2}, and a FF of 0.34.

In 2013, Bronstein *et al.* presented the synthesis and the characterization of two thiazole-containing conjugated polymers **P50** and **P51** that are isostructural to P3HT via the standard Grignard Metathesis reaction (GRIM)[71] polymerization.[23] ^{1}H NMR spectroscopy revealed that the regioregularity of the two polymers was lower than that typically obtained for P3HT. **P51** was 90% regioregular, while **P50** was found to be 93% regioregular. This was attributed to the lower relative solubility of the polymers during its synthesis, resulting in undesirable homo-coupling chain termination reactions. Polymers **P50** and **P51** both exhibited similar charge carrier mobilities of 0.02 cm^2.V^{-1}.s^{-1}, which were slightly lower than typically obtained for P3HT ($\sim$ 0.1 cm^2.V^{-1}.s^{-1}).[72] Solar cell devices were fabricated using a solution of the polymers with either PC$_{61}$BM, PC$_{71}$BM, or ICBA. The devices based on a blend of **P50**:PC$_{71}$BM yielded a maximum PCE value of 3.8% with a V_{OC} of 0.72 V, a J_{SC} of 10 mA.cm^{-2}, and a FF of 0.57. Replacing PC$_{71}$BM with ICBA as the acceptor slightly improved the V_{OC} to 0.59 V, however, decreased the J_{SC} to 8 mA.cm^{-2} and exhibiting an overall PCE of 3.8%. The use of **P51** as a donor and PC$_{61}$BM as an acceptor delivered even higher PCE of 4%, resulting in a notable V_{OC} of 0.82 V, a relative gain of >0.2 V in comparison to that of P3HT as a result of its deeper HOMO and a J_{SC} of 7.3 mA.cm^{-2}, and a FF of 0.66. Replacing PC$_{61}$BM with ICBA exhibited lower PCE of 2.7% and a significant reduction in both the J_{SC} (5.6 mA cm^{-2}) and FF (0.53) while resulting in the highest V_{OC} (1.0 V), making this

material combination particularly interesting for tandem solar cell applications. Table 4 provides a summary of the optoelectronic properties, energy levels, mobilities and photovoltaic properties of the polymers **P34-P51** shown in Figure 11 and 12.

Table 4. Summary of the optoelectronic properties, energy levels, mobilities and photovoltaic properties of the polymers **P34- P51** and **P69-70**.

	M_n [kDa]	PDI	E_g^{opt} [eV]	HOMO/LUMO [eV]	Max μ_h [cm^2.V^{-1}.s^{-1}]	J_{sc} [mA.cm^{-2}]	V_{oc} [V]	FF	PCE [%]	Ref.
P34	23.0	1.50	2.22	-5.33/-3.11	6×10^{-5}	-	-	-	-	56
P35	13.0	1.70	1.92	-5.39/-3.47	1.1×10^{-3}	-	-	-	-	56
P36	3.3	1.95	1.97	-5.15/-2.95	6.8×10^{-4}	7.84	0.86	0.57	3.82	58
P37	7.0	1.20	1.92	-5.19/-3.11	3.9×10^{-3}	10.3	0.78	0.46	3.71	60
P38	21.3	1.42	1.91	-5.26/-2.93	5.9×10^{-4}	7.18	0.82	0.50	2.92	60
P39	-	-	-	-	6.4 x 10^{-2}	-	-	-	-	62
P40	8.8	1.30	1.93	-5.50/-2.83	0.19	3.30	0.91	0.38	1.14	61
P41	7.5	1.50	1.99	-5.95/-2.63	1.8×10^{-3}	0.44	0.76	0.25	0.09	61
P42	6.9	1.40	1.94	-5.48/-2.92	0.18	6.64	0.82	0.47	2.54	61
P43	-	-	2.08	6.04/-3.04	-	-	-	-	-	63
P44	9.93	1.43	2.09	-6.02/-3.06	-	-	-	-	-	63
P45	-	-	2.05	-5.65/-3.60	-	10.9	0.81	0.57	5.06	64
P46	20.2	1.55	2.01	-5.16/-2.82	5.53×10^{-4}	5.20	0.88	0.61	2.81	65
P47	14.3	1.50	1.64	-5.24/-3.60	6.5×10^{-4}	1.02	0.68	0.21	0.15	66
P48	7.3	1.20	1.74	-5.53/-3.67	-	-	-	-	-	66
P49	6.4	1.07	1.98	-5.26/-3.26	7.9×10^{-5}	3.15	0.70	0.34	0.76	67
P50	21.0	2.20	1.90	-5.02/-3.12	2×10^{-2}	10.0	0.72	0.57	3.80	23
P51	27.0	1.80	1.90	-5.15/-3.25	2×10^{-2}	7.30	0.82	0.66	4.00	23
P69	22.2	1.98	1.89	-5.21/-3.25	7.11×10^{-3}	10.53	0.92	0.63	6.09	74
P70	43.0	1.72	1.71	-5.15/-3.45	1.1×10^{-3}	9.40	0.61	0.53	3.00	76

[a] electron mobility μ_e

Kim and co-workers reported three D-A thiophene/thiazole based semiconducting copolymers **P52**, **P53** and **P54** having identical backbones, but differing in the positioning of the alkyl side chain and the chain length.[73] Despite the differences in side chain lengths between the polymers, they display very similar absorption bands in solution and thin film. However, it was observed that as the length of the alkyl chains on the **P52-P54** backbone increases, the relative intensity of the shoulder peak decreases because of enhanced solubility, leading to reduced chain aggregation in solution. **P53** polymer film had a more pronounced shoulder peak, implying ordered $\pi - \pi$ stacking and a stronger inter-chain interaction in the thin-film state. Among the three polymers **P53** spin-coated film based OFET device exhibited the highest hole mobility of 0.25 $cm^2.V^{-1}.s^{-1}$. This was attributed to the strong interaction between adjacent polymer backbones as a result of the short π-π stacking distances.

The synthesis of dialkoxybithiazole (BTzOR) based polymers for OFET applications was reported by Marks, Facchetti and co-workers. Polymers **P55-P57** exhibited good solubilities, high crystallinity, extensive aggregation in solution, and low bandgaps ranging from 1.58-1.63 eV. Bottom-gate/top-contact OFETs fabricated from polymers **P55-P57** showed hole mobilities of 0.06-0.25 $cm^2.V^{-1}.s^{-1}$ and significantly enhanced current I_{on}/I_{off} ratios of 10^2-10^5.[19]

Early in 2014, Pammer *et al.* prepared head-to-tail regioregular poly(4-alkylthiazoles) **P58** and **P59** by Kumada-coupling polycondensation of 2,5-dihalogenated 4-alkylthiazoles.[12] The polymers were insoluble in organic solvents and could only be solubilized in the presence of trifluoro acetic acid (TFA) or boron trifluoride. To confirm the regioregularity of the polymers, the authors also synthesized an oligomeric model thiazole **M22**. The UV-vis absorption spectrum of **M22** was in good agreement with spectra measured for both **P58** and **P59**, providing convincing evidence for a highly regioregular head-to-tail structure. However, no OFET or OPV data was reported for the polymers. The same group later reported a modification to the structure of poly(4-alkylthiazoles) by synthesizing **P60**, **P61** and **P62** having a silyloxymethyl side-chain.[13] Once again it was found that **P60** and **P62** were relatively insoluble in common organic solvents, however, **P61** was fully soluble in hexane. The presence of the silyloxy side chains affects the solid state structure of the polymers which lead to a widened optical band gap with reduced π-stacking, in comparison to the

polythiazoles with alkyl substituents **P58** and **P59**. The performance of the polymers was not tested in organic electronic devices.
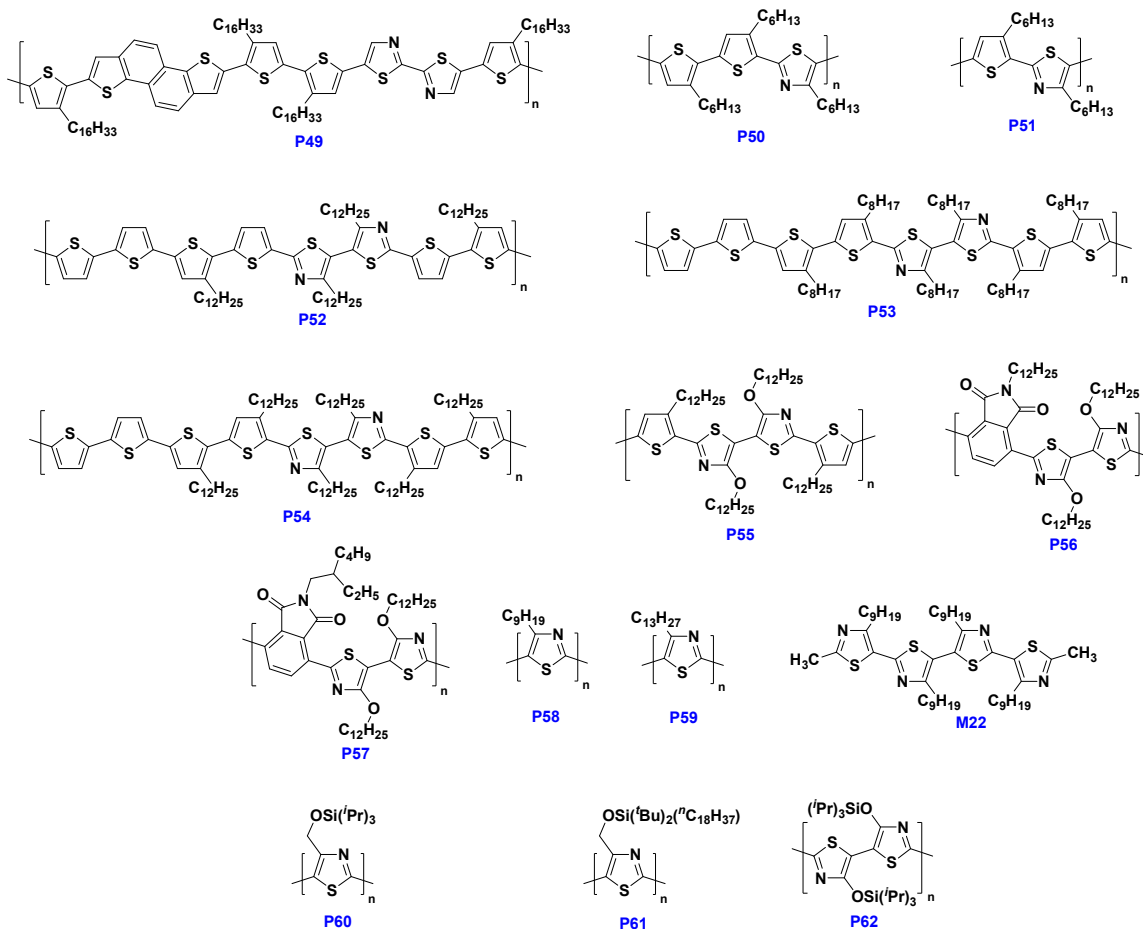

Figure 12- Chemical structure of bithiazole polymers **P49-P62** and small molecule **M22**.

In 2015, Kanbara and co-workers reported the synthesis of bithiazole-based copolymers containing electron-rich EDOT derivatives via Pd-catalyzed direct arylation.[74] The polycondenstion method resulted in polymers **P63-P65** having low molecular weights, owing to the low solubility of the polymers. The authors attributed this to the strong electrostatic interchain interactions between the polymer chains. No device data was reported for the polymers. However, the authors did state they are currently in progress and they compared the Pd-catalyzed direct arylation polycondensation to the conventional polycondensation via cross-coupling reactions and the dehalogenative

homocoupling reaction, declaring that the former method affords polymers with less waste via simplified synthetic steps.

Among the vast number of D-A copolymers, diketopyrrolopyrrole (DPP)-based copolymers have attracted extensive attention in organic electronics, owing to the fact that DPP derivatives can be easily synthesized and have excellent electrical properties. Reichmanis and co-workers in 2015 prepared the π-conjugated copolymer **P66**, containing dithienyldiketopyrrolopyrrole (DPPT) and bithiazole.[75] **P66** had a low optical bandgap (1.33 eV) and high electron affinities (-3.7 to -3.9 eV). The resulting, solution processable polymer **P66** showed electron mobilities as high as 0.3 cm^2.V^{-1}.s^{-1} with I_{On}/I_{Off} greater than 10^5 and a threshold voltage of 7.8 V in the bottom-contact/top-gate OFET configuration. There was negligible performance degradation after 4 months upon storing **P66** OFETs encapsulated by CYTOP (amorphous fluoropolymer) at 25 °C and 55-70% RH.
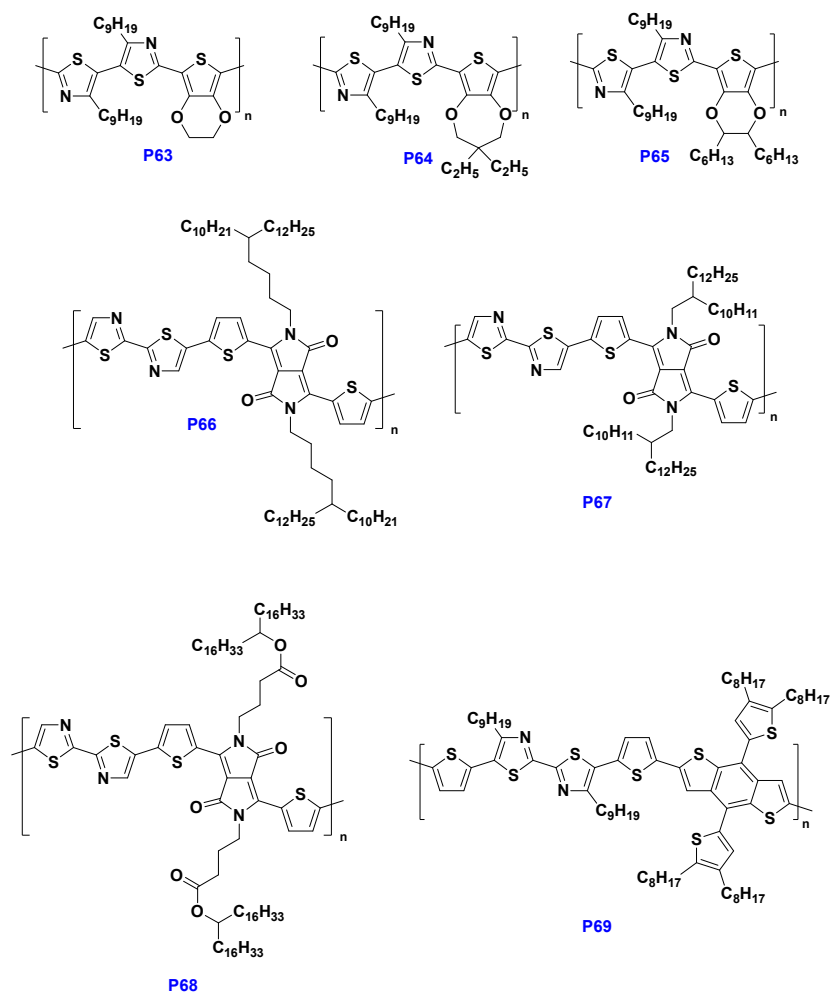
Figure 13- Chemical structure of bithiazole polymers **P63-P69**.

Recently, Li and co-workers synthesized bisthienyl diketopyrrolopyrrole-bithiazole based copolymers via two direct (hetero)arylation polymerization routes.[76] It was found that polymers prepared via direct (hetero)arylation polymerization from dibrominated bisthienyl DPP and 2,2'-bithiazole monomers (Route A) displayed better solubility, narrower molecular weight distributions and higher crystallinity in OTFT devices then that of the polymers synthesized from dibrominated 2,2'-bithiazole and bisthienyl DPP (Route B). The polymer **P67** prepared via Route A exhibited a maximum μ_e/μ_h of 0.53/0.06 cm^2.V^{-1}.s^{-1}, good current modulation (I_{on}/I_{off}) of 10^{5-6} for n-channel operation and of 10^6 for p-channel operation. The lower charge transport performance for polymer prepared from Route B as revealed by the UV-Vis and XRD data was attributed to the larger amount of irregular α–β coupling linkages and branched structures, as a result this causes reduced main chain conjugation length and contribute to the disorder of the polymer chains.

The same group recently designed a 2D-conjugated D–A copolymer **P69** by Stille coupling reaction based on bithienyl-benzodithiophene donor and bithiazole acceptor unit.[77] The **P69** copolymer was found to be highly coplanar, with a crystalline structure and low HOMO energy level (-5.21 eV) and a bandgap of 1.96 eV. The polymer exhibited typical p-type organic semiconductor characteristics with a hole mobility of 7.11×10^{-3} cm^2.V^{-1}.s^{-1}, and the best PCE of 6.09% with a high V_{OC} of 0.92 V, a J_{SC} of 10.53 mA.cm^{-2}, and a FF of 0.63. The achieved high V_{OC} values are the result of the low lying HOMO energy level of the **P69** copolymer. Table 5 provides a summary of the optoelectronic properties, energy levels, and mobilities of the polymers shown in Figure 12 and 13.

Table 5. Summary of the optoelectronic properties, energy levels, mobilities and photovoltaic properties of the polymers **P52-P68**.

	M_n	PDI	E_g^{opt} [eV]	HOMO/LUMO [eV]	Max μ_h [cm^2.V^{-1}.s^{-1}]	Ref.
P52	16.3	2.07	2.03	-5.25/-3.22	2×10^{-3}	70
P53	14.2	2.14	1.96	-5.01/-3.05	0.25	70
P54	15.1	1.85	1.95	-5.00/-3.05	9.7×10^{-2}	70
P55	11.7	2.00	1.63	-4.94/-3.31	0.25	19
P56	5.2	3.20	1.62	-5.18/-3.56	6×10^{-2}	19
P57	34.6	3.70	1.58	-5.16/-3.58	0.13	19
P66	64.0	3.60	1.33	-5.54/-3.75	0.3 ^{a}	72
P67	18.0	3.80	1.42	-5.56/-3.63	6×10^{-2} 0.53 ^{a}	73
P68	11.0	2.50	1.50	-	3.3×10^{-3a}	73

^{a} electron mobility μ_e

Fused bithiazole containing semiconductors

The inclusion of large fused aromatic building blocks has been established as a popular approach to reduce rotational disorder along the conjugated polymer backbone. Rigid and coplanar polymer backbones have been shown to significantly improve charge transport and device performances. However from a chemical point of view, the introduction of bridging atoms between aromatic rings provides a synthetic handle to further tune the opto-electronic properties as well as optimize the material processability. Inspired by the excellent processability and superior device performance of dithieno[3,2-*b*:2′,3′-*d*]pyrrole (**M23-M26**) containing polymers (Figure 14), Al-Hashimi *et al*. synthesised the thiazole analogue, pyrrolo[3,2-*d*:4,5-*d'*]bisthiazole (**M24**).[78] By flanking the central pyrrole moiety with thiazole units, the ionization potential of the resulting polymers could be lowered (by ~0.5 eV), making the **M24** containing polymers significantly more stable to oxidation under ambient conditions. Thiazole containing polymers tend to be less soluble than their thiophene containing counter-parts, which is why the bridging nitrogen atom was substituted with a long branched 2-octyl-dodecyl chain to ensure sufficient solubility. The authors

synthesized four **M24** containing polymers with high molecular weights and excellent solubility. By copolymerizing the **M24** unit with different thiophene derivatives, the HOMO energy level could be gradually adjusted from -5.15 eV to -5.30 eV. Compared to the **M24** containing polymers, the UV-*vis.* absorption spectra of the **M24** polymers were significantly red-shifted, highlighting the planar backbone structure with enhanced electron delocalization of thiazole containing polymers. When incorporated into OFET devices, the **P70** polymer (Figure 15) achieved saturated hole mobilities of 1.1×10^{-3} $cm^2.V^{-1}.s^{-1}$. When used as donor material in fullerene ($PC_{71}BM$) BHJ solar cells, the good polymer solubility yielded high quality films with very low root mean square roughness (<1 nm).[79] As indicated in Table 4 the best device performance (PCE = 3.0%) was achieved at higher fullerene loadings (**P70**: $PC_{71}BM$ 1:3.5). Due to the low lying HOMO energy level, the V_{oc} (0.61 V) of the **P70** device was larger than for a comparable device employing P3HT as donor material. However due to the low photocurrent (9.4 mA/cm^2), the overall device performance was lacking the P3HT device (3.9%).
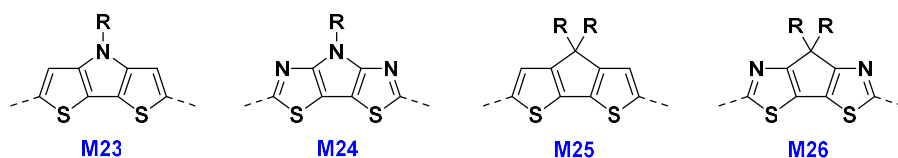

Figure 14: Chemical structures of common fused bithiophene and bithiazole monomers **M23-M26.**

Scherf and co-workers took a similar approach by bridging the bithiazole moiety with carbon (**M26**).[80] In contrast to the aforementioned **M23** with its nitrogen bridge, the sp^3-hybridized carbon bridge in **M26** allows to attach two alkyl chains per bridging atom, making the use of bulky branched alkyl side chains obsolete. The authors prepared several **M26** containing low-bandgap polymers, whereby the copolymer with naphthalene-1,4,5,8-tetracarboxylic-*N,N'*-bis(2-octyldodecyl)diimide (**P71**) was the most interesting one. Compared to the cyclopentadithiophene (**M25**) building block, **M26** is a weaker donor, which is reflected by a hypsochromic shift of >100 nm in the UV-*vis.* absorption of **P71** compared to the **P72** polymer. Unfortunately, no devices were prepared, which would have made for an interesting comparison between both materials,

especially considering the very low lying HOMO energy level of **P71** (-5.95 eV) which might have yielded high V_{oc} values in OPV devices.

Aso *et al.* were as well interested in carbon bridged bithiazole, but instead of alkylating the bridging carbon, they synthesized fused thiazole derivatives bridged by carbonyl.[81] In contrast to bithiazole derivatives, the carbonyl bridged moiety has a significantly lower bandgap (0.6 eV), due to a substantial decrease in LUMO energy level. The carbonyl bridged bithiazole (**M27**) unit was flanked with 2,2,2-trifluoroacetophenone in order to obtain a new highly crystalline n-type semiconductor. Single crystal x-ray diffraction studies revealed several short contacts between adjacent molecules, induced by the carbonyl bridge, resulting in a dense packing structure with short (< 3.5Å) interplanar distances. As a result of the dense packing motif and the resulting large transfer integrals, electron mobilities of up to 0.06 $cm^2.V^{-1}.s^{-1}$ were measured in OFET. Remarkably, **M27** device showed excellent ambient stability due to the low lying LUMO and no significant device degradation was observed when operated in air. In contrast, the bithiazole analogue (**M28**) achieved only modest electron mobilities (2×10^{-3} $cm^2.V^{-1}.s^{-1}$) under vacuum and no transistor characteristics could be measured under ambient operating conditions.
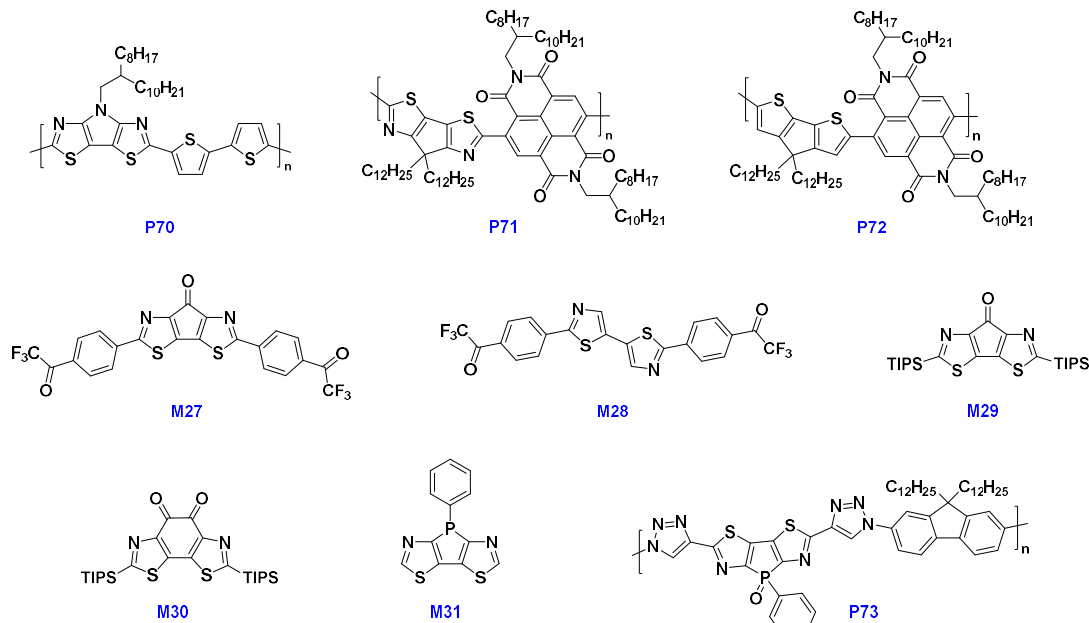

Figure 15: Chemical structures of organic semiconductors comprising of fused-bithiazole/bithiophene and bithiazole **M28** moieties.

In 2011, the Marder group extended the bridging concept on bithiazole moieties further and synthesized a fused system with a dicarbonyl bridge.[82] By introducing a α-dicarbonyl bridge, the frontier energy levels could be further lowered. Compared to the mono-carbonyl bridged bithiazole (**M29**) derivative, the LUMO energy level could be lowered by an additional 0.2 eV (**M30**) in case of the dicarbonyl bridge. Due to the increased electron affinity, the bicarbonyl derivatives should be substantially more stable under ambient conditions, making it potentially a promising building block for air-stable n-type semiconductors. Due to the structural resemblance between **M29** and **M30**, both compounds show similar packing motifs in single crystal x-ray diffraction experiments with short intermolecular π-stacking distances and S---O contacts.

The bithiazole building block however is not only of interest for air-stable n-type semiconductors, but some derivatives showed promising emissive properties.[83] Baumgartner and co-workers were interested in combining the excellent photophysical properties of dithienophosphole with the high electron affinity of thiazole based building blocks. The introduction of phosphorus as the bridging element into bithiazole is expected to further stabilize the LUMO energy via σ*-π* orbital coupling interactions, previously demonstrated in phosphole containing derivatives.[84] The synthesized dithiazolophosphole derivatives (**M31**) proved extremely versatile and several chemical modifications were performed on the phosphorus bridge, *i.e.* oxidation, sulfuration, complexations with Au. The tricyclic dithiazolophosphole unit was as well introduced into polymers (**P73**) via Huisgen alkynyl-azide click reaction.[83] Unfortunately, the polymer showed rather weak emissive properties, however proved to be a promising candidate for selective colorimetric and fluorescent Cu[II] sensing. The dithiazolophosphole moiety showed some promising properties, but further studies, as well as optimized polymersization conditions will be needed to elucidate the full potential of this intriguing building block.

Theoretical design of new fused bithiazole containing electron deficient polymers

Density functional theory calculations have been established as a powerful tool to design new conjugated polymers and to estimate certain physical properties, before embarking on the tedious chemical synthesis. We designed a couple of acceptor building blocks to be polymerized with the fused bithiazole building block in order to obtain high performance acceptor polymers for use in bulk heterojunction solar cells and as organic field effect transistors. In order to validate our

approach, we took advantage of DFT calculations to predict geometric, electronic and optical properties of five potential acceptors moieties, and prior to the synthesis of the polymers.
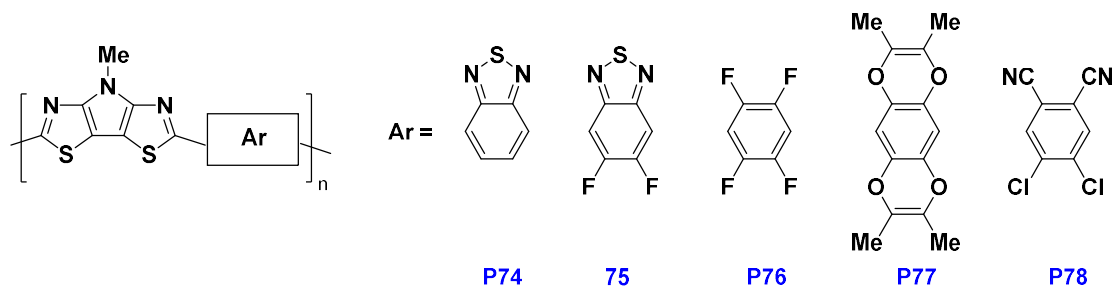

Figure 16: Molecular structures of five proposed copolymers, which contain common PBTz unit in combination with different chromophores (π) **P74-P78**.

To investigate the electronic and optical properties of the five theoretically proposed polymers, DFT and time dependent (TD)-DFT calculations were carried out on models based on 4-methyl-4H-pyrrolo[2,3-*d*:5,4-*d*]bis(thiazole) (PBTz) unit copolymerized with five different chromophores (Figure 11), by using the Gaussian 09 software.[85] These specific chromophores we refer to are benzo[*c*][1,2,5]thiadiazole (BT; **P74**), 5,6-difluorobenzo[*c*][1,2,5]thiadiazole (**P75**), 1,2,4,5-tetrafluorobenzene (**P76**), 2,3,7,8-tetramethylbenzo[1,2-*b*:4,5-*b*]bis([1,4]dioxine) (**P77**), and 4,5-dichlorophtalonitrile (**P78**). In all cases, the substituents on PBTz units, as well as on the second unit of **P77**, are represented by methyl groups in order to reduce computational burden. It has been shown that modeling the electronic structure of polymers with long-chain alkyl groups by replacing it with methyl groups does not affect the frontier orbitals, but in cases of excessive steric accumulation it could affect their planarity.[86] Since the frontier orbitals are precisely those of interest in DFT modelling, we analyzed HOMO and LUMO wave-functions of these polymers. In Figure 11, we present optimized (S₀) geometries of five polymers as determined at the HSE06/6-31G (d,p) level with periodic boundary conditions (PBC), placing the HOMO and LUMO spatial distributions over the single repeating unit.[87-90] The analysis reveals that both HOMO and LUMO orbitals are well delocalized over the whole π-system in all cases, and neither has contribution from the methyl groups. The polymers **P75**, **P76**, and **P78** exhibit a highly planar structure with dihedral angles between consecutive units that are very close to zero. On the other hand, **P74** and **P77** slightly deviate from planarity with the dihedral angles of 21.0° and 11.2°, respectively.
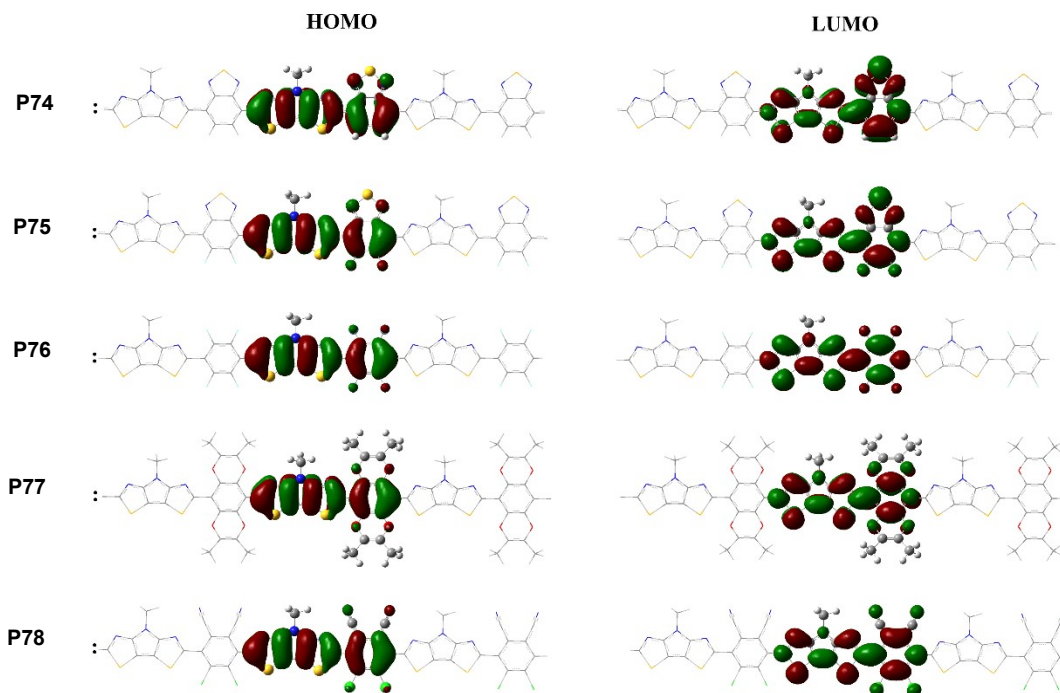
Figure 17: Optimized ground-state (S_0) geometric structures of five polymers (**P74-P78**) calculated at the HSE06/6-31(d,p) level with periodic boundary conditions (PBC). HOMO and LUMO wave-functions are placed over a single repeat unit for the sake of clarity.

To study the influence of the terminal acceptor, we utilized fused bithiazole as the core unit and five different chromophores as the conjugated bridge. The computed bandgaps for the five polymers range between 1.24 to 1.94 eV as depicted in Figure 17 and 18. Over the past few years, one of the most significant advances in the field of polymer solar cells has be the synthesis of fluorinated polymers based on the electron-deficient BT moiety, which lack the solid working principles of previous designs, but have a positive effect on the power conversion efficiency. To evaluate the influence of having a fluorinated BT unit on the charge-transport characteristics in organic field-effect transistors we calculated the HOMO/LUMO energy levels for non-fluorinated analogue **P74** and its difluorinated BT-based polymer **P75**. The difference that was observed as a result of having the fluorine in the polymer backbone was the shifting of both the HOMO and LUMO energy levels towards the negative potentials, which in turn is reflected in the reduction of the bandgap of **P75** (1.38 *vs* 1.24 eV). This might also be the consequence of higher planarity of **P75**. In contrast, further exchange of N-S-N sequence of BT (**P75**), with additional two fluorine atoms, which results in structural change of the chromophore's aromatic core, changing it from

benzothiadiazole into the phenyl ring, leading to an increased bandgap in **P76** (1.79 eV). In polymer **P77**, the nature of the substituents on the phenyl ring have been changed by selecting one specific electron-rich chromophore as an acceptor building block. The frontier orbitals of the polymer are pinned at the less negative potentials as compared with other polymers, with substantial destabilization of LUMO, owing to the electron-donating nature of the oxygen-containing substituents on phenyl rings. This polymer has the largest bandgap of the series (1.94 eV), which is also affected by its small deviation from planarity. **P78** has the most stabilized orbitals that is likely caused by their extension over the CN-substituent, with the calculated bandgap of 1.64 eV (Figure 18).
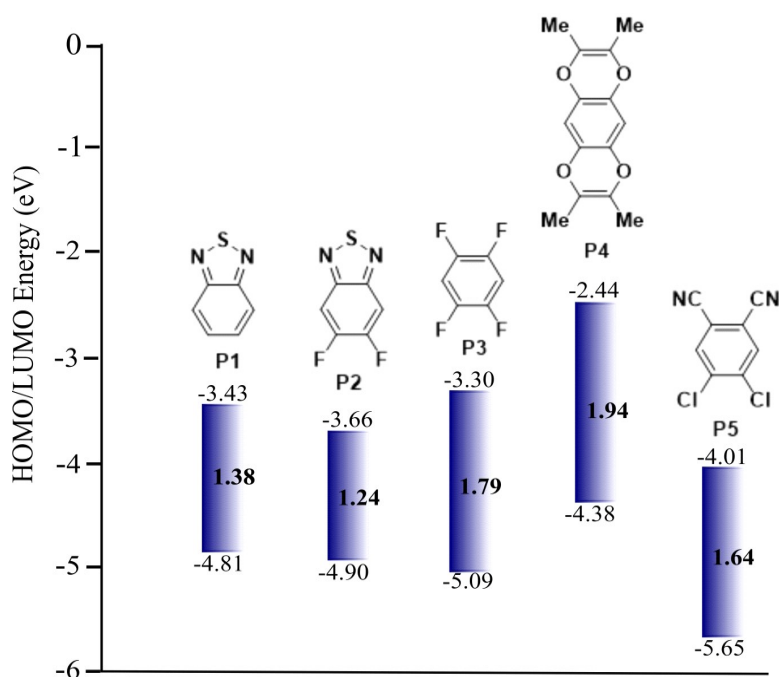

Figure 18: HOMO (bottom of rectangles) and LUMO (top of rectangles) energies (eV) with appropriate band gaps (inside the rectangles) of five polymers.

The maximum absorption wavelengths (λ_{max}) as vertical transition energies, oscillator strengths (f), as well as the nature of the transitions associated with S_0 S_1 in $CHCl_3$ were obtained by TD-DFT, and summarized in Table 1. This was calculated at the CAM-B3LYP/6-31+G(d,p) level of theory, based on the HSE06/6-31G(d,p) optimized geometries of appropriate tetramers.[91] Validity of the functional/basis set choice for the prediction of the spectra has been corroborated previously.[92] The spectra of **T1-T5** display one main lower-energy transition with a large oscillator

strength (f) (Table 6) that is accompanied by the series of higher-energy transitions with very small oscillator strengths (not presented in the Table 6). The absorption maxima (λ_{max}) for **T1-T5**, which arise from S_0 S_1, mainly originate from electron transition from HOMO to LUMO, but it also has contribution from HOMO-1 to the LUMO+1 electron promotion (Table 6). The conclusion is that the small change in the molecular structure of the chromophores, by introducing different electron-withdrawing or donating substituents, may considerably influence both band gaps and λ_{max} (as well as corresponding oscillator strengths as a reflection of molar extinction coefficients).

Table 6. Calculated vertical transition energies (E, eV), maximum absorption wavelengths (λ_{max}, nm), oscillator strengths (f), and electronic configurations for the S_0 S_1 excitation.

Tetramer	Excitation	E_g (eV)	λ_{max} (nm)	f	Electronic configuration
T1	S_0 S_1	2.12	585	4.62	H L (69%) H-1 L+1 (16%)
T2	S_0 S_1	1.99	622	5.22	H L (72%) H-1 L+1 (15%)
T3	S_0 S_1	2.50	497	6.04	H L (69%) H-1 L+1 (16%)
T4	S_0 S_1	2.60	477	5.93	H L (67%) H-1 L+1 (15%)
T5	S_0 S_1	2.33	532	5.81	H L (65%) H-1 L+1 (13%)

H and L represent HOMO and LUMO orbitals, respectively.

Conclusion

In this review we discussed the tremendous progress made over the past two decades to incorporate the electron deficient thiazole building block into organic semiconductors. We summarized the design rationale behind more than 100 different thiazole based structures and the effects on device performances in BHJ solar cells and OFET devices. In contrast to thiophene containing semiconductors, the thiazole counter-parts show significantly improved lifetimes under ambient operating conditions, due to the lower lying frontier energy levels. Furthermore, the presence of the lone pair on the nitrogen in the thiazole ring has been shown to open-up additional design avenues to further planarize the conjugated building blocks due to a "conformational lock" mechanism between the lone pair and the antibonding orbitals in adjacent aromatic ring.

Thiazole based organic semiconductors are sometimes struggling to outperform thiophene based OSC, however the improved oxidative stability and lower lying energy levels present attractive features to develop new and air-stable n-type semiconductors. This is particularly true considering the breadth of chemical modifications still unexplored on the thiazole unit and the facile synthesis by which they could be performed. Now that the development of electron-rich thiophene based semiconductors is slowing, the research focus will shift towards the synthesis of higher performing, air-stable n-type semiconductors, thus undoubtedly shifting thiazole based materials into the spot-light.

Acknowledgment

References

1.   X. G. Guo, A. Facchetti and T. J. Marks, *Chem Rev*, 2014, **114**, 8943-9021.
2.   C. J. Brabec, S. Gowrisanker, J. J. M. Halls, D. Laird, S. J. Jia and S. P. Williams, *Adv Mater*, 2010, **22**, 3839-3856.
3.   G. Dennler, M. C. Scharber and C. J. Brabec, *Adv Mater*, 2009, **21**, 1323-1338.
4.   C. J. Brabec, A. Cravino, D. Meissner, N. S. Sariciftci, T. Fromherz, M. T. Rispens, L. Sanchez and J. C. Hummelen, *Adv Funct Mater*, 2001, **11**, 374-380.
5.   A. Tada, Y. F. Geng, Q. S. Wei, K. Hashimoto and K. Tajima, *Nat Mater*, 2011, **10**, 450-455.
6.   A. Facchetti, *Chem Mater*, 2011, **23**, 733-758.
7.   L. Y. Lu, T. Y. Zheng, Q. H. Wu, A. M. Schneider, D. L. Zhao and L. P. Yu, *Chem Rev*, 2015, **115**, 12666-12731.
8.   H. W. Hu, K. Jiang, G. F. Yang, J. Liu, Z. K. Li, H. R. Lin, Y. H. Liu, J. B. Zhao, J. Zhang, F. Huang, Y. Q. Qu, W. Ma and H. Yan, *J Am Chem Soc*, 2015, **137**, 14149-14157.
9.   Y. L. J. Zhao, G. Yang, K. Jiang, H. Lin, H. Ade, W. Ma and H. Yan, Nature Energy, 2016, 1, 15027.
10.   S. Holliday, J. E. Donaghey and I. McCulloch, *Chem Mater*, 2014, **26**, 647-663.
11.   H. Sirringhaus, *Adv Mater*, 2014, **26**, 1319-1335.
12.   F. Pammer and U. Passlack, *Acs Macro Lett*, 2014, **3**, 170-174.
13.   F. Pammer, J. Jager, B. Rudolf and Y. Sun, *Macromolecules*, 2014, **47**, 5904-5912.
14.   R. P. Ortiz, H. Yan, A. Facchetti and T. J. Marks, *Materials*, 2010, **3**, 1533-1558.
15.   Y. Z. Lin, H. J. Fan, Y. F. Li and X. W. Zhan, *Adv Mater*, 2012, **24**, 3087-3106.
16.   C. L. Wang, H. L. Dong, W. P. Hu, Y. Q. Liu and D. B. Zhu, *Chem Rev*, 2012, **112**, 2208-2267.
17.   K. Oniwa, H. Kikuchi, T. Kanagasekaran, H. Shimotani, S. Ikeda, N. Asao, Y. Yamamoto, K. Tanigaki and T. Jin, *Chem Commun*, 2016, **52**, 4926-4929.
18.   T. L. D. Tam and T. T. Lin, *Macromolecules*, 2016, **49**, 1648-1654.
19.   X. G. Guo, J. Quinn, Z. H. Chen, H. Usta, Y. Zheng, Y. Xia, J. W. Hennek, R. P. Ortiz, T. J. Marks and A. Facchetti, *J Am Chem Soc*, 2013, **135**, 1986-1996.
20.   Z. Li, J. F. Ding, N. H. Song, J. P. Lu and Y. Tao, *J Am Chem Soc*, 2010, **132**, 13160-13161.

21. L. Ying, B. B. Y. Hsu, H. M. Zhan, G. C. Welch, P. Zalar, L. A. Perez, E. J. Kramer, T. Q. Nguyen, A. J. Heeger, W. Y. Wong and G. C. Bazan, *J Am Chem Soc*, 2011, **133**, 18538-18541.

22. H. H. Cho, T. E. Kang, K. H. Kim, H. Kang, H. J. Kim and B. J. Kim, *Macromolecules*, 2012, **45**, 6415-6423.

23. H. Bronstein, M. Hurhangee, E. C. Fregoso, D. Beatrup, Y. W. Soon, Z. G. Huang, A. Hadipour, P. S. Tuladhar, S. Rossbauer, E. H. Sohn, S. Shoaee, S. D. Dimitrov, J. M. Frost, R. S. Ashraf, T. Kirchartz, S. E. Watkins, K. Song, T. Anthopoulos, J. Nelson, B. P. Rand, J. R. Durrant and I. McCulloch, *Chem Mater*, 2013, **25**, 4239-4249.

24. W. J. Li, H. E. Katz, A. J. Lovinger and J. G. Laquindanum, *Chem Mater*, 1999, **11**, 458-465.

25. J. Cao, J. W. Kampf and M. D. Curtis, *Chem Mater*, 2003, **15**, 404-411.

26. H. Moon, W. S. Jahng and M. D. Curtis, *J Mater Chem*, 2008, **18**, 4856-4863.

27. S. Ando, J. Nishida, E. Fujiwara, H. Tada, Y. Inoue, S. Tokito and Y. Yamashita, *Chem Lett*, 2004, **33**, 1170-1171.

28. S. Ando, R. Murakami, J. Nishida, H. Tada, Y. Inoue, S. Tokito and Y. Yamashita, *J Am Chem Soc*, 2005, **127**, 14996-14997.

29. P. Dutta, W. Yang, W. H. Lee, I. N. Kang and S. H. Lee, *J Mater Chem*, 2012, **22**, 10840-10851.

30. Y. Z. Lin, P. Cheng, Y. Liu, Q. Q. Shi, W. P. Hu, Y. F. Li and X. W. Zhan, *Org Electron*, 2012, **13**, 673-680.

31. S. Guo, J. Ning, V. Korstgens, Y. Yao, E. M. Herzig, S. V. Roth and P. Muller-Buschbaum, *Adv Energy Mater*, 2015, **5**.

32. H. X. Zhou, L. Q. Yang, A. C. Stuart, S. C. Price, S. B. Liu and W. You, *Angew Chem Int Edit*, 2011, **50**, 2995-2998.

33. M. F. Calhoun, J. Sanchez, D. Olaya, M. E. Gershenson and V. Podzorov, *Nat Mater*, 2008, **7**, 84-89.

34. H. Usta, W. C. Sheets, M. Denti, G. Generali, R. Capelli, S. F. Lu, X. G. Yu, M. Muccini and A. Facchetti, *Chem Mater*, 2014, **26**, 6542-6556.

35. J. I. Lee, G. Klaerner and R. D. Miller, *Chem Mater*, 1999, **11**, 1083-1088.

36. H. J. Cho, B. J. Jung, N. S. Cho, J. Lee and H. K. Shim, *Macromolecules*, 2003, **36**, 6704-6710.

37. J. Lee, B. J. Jung, S. K. Lee, J. I. Lee, H. J. Cho and H. K. Shim, *J Polym Sci Pol Chem*, 2005, **43**, 1845-1857.

38. I. H. Jung, Y. K. Jung, J. Lee, J. H. Park, H. Y. Woo, J. I. Lee, H. Y. Chu and H. K. Shim, *J Polym Sci Pol Chem*, 2008, **46**, 7148-7161.

39. D. D. Cunningham, A. Galal, C. V. Pham, E. T. Lewis, A. Burkhardt, L. Lagurendavidson, A. Nkansah, O. Y. Ataman, H. Zimmer and H. B. Mark, *J Electrochem Soc*, 1988, **135**, 2750-2754.

40. A. Berlin, E. Brenna, G. A. Pagani, F. Sannicolo, G. Zotti and G. Schiavon, *Synthetic Met*, 1992, **51**, 287-297.

41. G. Zotti, G. Schiavon, A. Berlin, G. Fontana and G. Pagani, *Macromolecules*, 1994, **27**, 1938-1942.

42. K. C. Li, J. H. Huang, Y. C. Hsu, P. J. Huang, C. W. Chu, J. T. Lin, K. C. Ho, K. H. Wei and H. C. Lin, *Macromolecules*, 2009, **42**, 3681-3693.

43. J. H. Huang, K. C. Li, F. C. Chien, Y. S. Hsiao, D. Kekuda, P. L. Chen, H. C. Lin, K. C. Ho and C. W. Chu, *J Phys Chem C*, 2010, **114**, 9062-9069.

44. D. Patra, D. Sahu, H. Padhy, D. Kekuda, C. W. Chu and H. C. Lin, *J Polym Sci Pol Chem*, 2010, **48**, 5479-5489.

45. M. J. Zhang, H. J. Fan, X. Guo, Y. J. He, Z. G. Zhang, J. Min, J. Zhang, G. J. Zhao, X. W. Zhan and Y. F. Li, *Macromolecules*, 2010, **43**, 5706-5712.

46. J. H. Huang, F. C. Chen, C. L. Chen, A. T. Huang, Y. S. Hsiao, C. M. Teng, F. W. Yen, P. L. Chen and C. W. Chu, *Org Electron*, 2011, **12**, 1755-1762.

47. M. J. Zhang, X. Guo and Y. F. Li, *Macromolecules*, 2011, **44**, 8798-8804.

48.   H. L. Zheng, C. T. Gu, Q. Q. Zhu, X. C. Bao, S. G. Wen, M. Qiu, D. Q. Zhu, M. L. Sun and R. Q. Yang, *J Appl Polym Sci*, 2015, **132**.

49.   I. H. Jung, J. Yu, E. Jeong, J. Kim, S. Kwon, H. Kong, K. Lee, H. Y. Woo and H. K. Shim, *Chem-Eur J*, 2010, **16**, 3743-3752.

50.   X. R. Zhang, H. Bronstein, A. J. Kronemeijer, J. Smith, Y. Kim, R. J. Kline, L. J. Richter, T. D. Anthopoulos, H. Sirringhaus, K. Song, M. Heeney, W. M. Zhang, I. McCulloch and D. M. DeLongchamp, *Nat Commun*, 2013, **4**.

51.   M. J. Zhang, X. Guo, X. C. Wang, H. Q. Wang and Y. F. Li, *Chem Mater*, 2011, **23**, 4264-4270.

52.   W. Y. Wong, X. Z. Wang, Z. He, K. K. Chan, A. B. Djurisic, K. Y. Cheung, C. T. Yip, A. M. C. Ng, Y. Y. Xi, C. S. K. Mak and W. K. Chan, *J Am Chem Soc*, 2007, **129**, 14372-14380.

53.   B. L. Lee, K. M. Han, E. K. Lee, I. N. Kang, D. H. Kim and S. Lee, *Synthetic Met*, 2009, **159**, 132-136.

54.   D. H. Kim, B. L. Lee, H. Moon, H. M. Kang, E. J. Jeong, J. I. Park, K. M. Han, S. Lee, B. W. Yoo, B. W. Koo, J. Y. Kim, W. H. Lee, K. Cho, H. A. Becerril and Z. Bao, *J Am Chem Soc*, 2009, **131**, 6124-6132.

55.   M. J. Zhang, H. J. Fan, X. Guo, Y. Yang, S. S. Wang, Z. G. Zhang, J. Zhang, X. W. Zhan and Y. F. Li, *J Polym Sci Pol Chem*, 2011, **49**, 2746-2754.

56.   X. Guo, M. J. Zhang, L. J. Huo, C. H. Cui, Y. Wu, J. H. Hou and Y. F. Li, *Macromolecules*, 2012, **45**, 6930-6937.

57.   J. Y. Liu, R. Zhang, I. Osaka, S. Mishra, A. E. Javier, D. M. Smilgies, T. Kowalewski and R. D. McCullough, *Adv Funct Mater*, 2009, **19**, 3427-3434.

58.   D. Patra, D. Sahu, H. Padhy, D. Kekuda, C. W. Chu, K. H. Wei and H. C. Lin, *Macromol Chem Phys*, 2011, **212**, 1960-1970.

59.   S. Paek, J. Lee, H. S. Lim, J. Lim, J. Y. Lee and C. Lee, *Synthetic Met*, 2010, **160**, 2273-2280.

60.   J. H. Hou, Z. A. Tan, Y. Yan, Y. J. He, C. H. Yang and Y. F. Li, *J Am Chem Soc*, 2006, **128**, 4911-4916.

61.   M. J. Zhang, H. J. Fan, X. Guo, Y. J. He, Z. G. Zhang, J. Min, J. Zhang, G. J. Zhao, X. W. Zhan and Y. F. Li, *Macromolecules*, 2010, **43**, 8714-8717.

62.   H. J. Fan, M. J. Zhang, X. Guo, Y. F. Li and X. W. Zhan, *Acs Appl Mater Inter*, 2011, **3**, 3646-3653.

63.   P. Shen, H. J. Bin, X. W. Chen and Y. F. Li, *Org Electron*, 2013, **14**, 3152-3162.

64.   Q. Q. Shi, H. J. Fan, Y. Liu, J. M. Chen, L. C. Ma, W. P. Hu, Z. G. Shuai, Y. F. Li and X. W. Zhan, *Macromolecules*, 2011, **44**, 4230-4240.

65.   Y. Liu, Q. Q. Shi, L. C. Ma, H. L. Dong, J. H. Tan, W. P. Hu and X. W. Zhan, *J Mater Chem C*, 2014, **2**, 9505-9511.

66.   H. F. Wang, Q. Q. Shi, Y. Z. Lin, H. J. Fan, P. Cheng, X. W. Zhan, Y. F. Li and D. B. Zhu, *Macromolecules*, 2011, **44**, 4213-4221.

67.   X. L. Zhao, D. L. Yang, H. Y. Lv, L. Yin and X. N. Yang, *Polym Chem-Uk*, 2013, **4**, 57-60.

68.   M. J. Zhang, Y. P. Sun, X. Guo, C. H. Cui, Y. J. He and Y. F. Li, *Macromolecules*, 2011, **44**, 7625-7631.

69.   B. Balan, C. Vijayakumar, A. Saeki, Y. Koizumi and S. Seki, *Macromolecules*, 2012, **45**, 2709-2719.

70.   P. Dutta, H. Park, M. Oh, S. Bagde, I. N. Kang and S. H. Lee, *J Polym Sci Pol Chem*, 2013, **51**, 2948-2958.

71.   R. S. Loewe, P. C. Ewbank, J. S. Liu, L. Zhai and R. D. McCullough, *Macromolecules*, 2001, **34**, 4324-4333.

72.   H. Sirringhaus, P. J. Brown, R. H. Friend, M. M. Nielsen, K. Bechgaard, B. M. W. Langeveld-Voss, A. J. H. Spiering, R. A. J. Janssen, E. W. Meijer, P. Herwig and D. M. de Leeuw, *Nature*, 1999, **401**, 685-688.

73.   J. Lee, J. W. Chung, J. Jang, D. H. Kim, J. I. Park, E. Lee, B. L. Lee, J. Y. Kim, J. Y. Jung, J. S. Park, B. Koo, Y. W. Jin and D. H. Kim, *Chem Mater*, 2013, **25**, 1927-1934.

74.   W. Lu, J. Kuwabara, M. Kuramochi and T. Kanbara, *J Polym Sci Pol Chem*, 2015, **53**, 1396-1402.

75.   B. Y. Fu, C. Y. Wang, B. D. Rose, Y. D. Jiang, M. Chang, P. H. Chu, Z. B. Yuan, C. Fuentes-Hernandez, B. Kippelen, J. L. Bredas, D. M. Collard and E. Reichmanis, *Chem Mater*, 2015, **27**, 2928-2937.
76.   C. Guo, J. Quinn, B. Sun and Y. N. Li, *Polym Chem-Uk*, 2016, **7**, 4515-4524.
77.   K. Wang, X. Guo, B. Guo, W. B. Li, M. J. Zhang and Y. F. Li, *Macromol Rapid Comm*, 2016, **37**, 1066-1073.
78.   M. Al-Hashimi, J. G. Labram, S. Watkins, M. Motevalli, T. D. Anthopoulos and M. Heeney, *Organic Letters*, 2010, **12**, 5478-5481.
79.   R. Xia, M. Al-Hashimi, W. C. Tsoi, M. Heeney, D. D. C. Bradley and J. Nelson, *Solar Energy Materials and Solar Cells*, 2012, **96**, 112-116.
80.   C. J. Kudla, D. Dolfen, K. J. Schottler, J.-M. Koenen, D. Breusov, S. Allard and U. Scherf, *Macromolecules*, 2010, **43**, 7864-7867.
81.   Y. Ie, M. Nitani, M. Karakawa, H. Tada and Y. Aso, *Advanced Functional Materials*, 2010, **20**, 907-913.
82.   Y. A. Getmanenko, C. Risko, P. Tongwa, E.-G. Kim, H. Li, B. Sandhu, T. Timofeeva, J.-L. Brédas and S. R. Marder, *The Journal of Organic Chemistry*, 2011, **76**, 2660-2671.
83.   X. He, A. Y. Y. Woo, J. Borau-Garcia and T. Baumgartner, *Chemistry – A European Journal*, 2013, **19**, 7620-7630.
84.   T. Baumgartner and R. Réau, *Chemical Reviews*, 2006, **106**, 4681-4727.
85.   M. J. Frisch, G. W. Trucks, H. B. Schlegel, G. E. Scuseria, M. A. Robb, J. R. Cheeseman, G. Scalmani, V. Barone, B. Mennucci, G. A. Petersson, H. Nakatsuji, M. Caricato, X. Li, H. P. Hratchian, A. F. Izmaylov, J. Bloino, G. Zheng, J. L. Sonnenberg, M. Hada, M. Ehara, K. Toyota, R. Fukuda, J. Hasegawa, M. Ishida, T. Nakajima, Y. Honda, O. Kitao, H. Nakai, T. Vreven, J. A. Montgomery Jr., J. E. Peralta, F. Ogliaro, M. J. Bearpark, J. Heyd, E. N. Brothers, K. N. Kudin, V. N. Staroverov, R. Kobayashi, J. Normand, K. Raghavachari, A. P. Rendell, J. C. Burant, S. S. Iyengar, J. Tomasi, M. Cossi, N. Rega, N. J. Millam, M. Klene, J. E. Knox, J. B. Cross, V. Bakken, C. Adamo, J. Jaramillo, R. Gomperts, R. E. Stratmann, O. Yazyev, A. J. Austin, R. Cammi, C. Pomelli, J. W. Ochterski, R. L. Martin, K. Morokuma, V. G. Zakrzewski, G. A. Voth, P. Salvador, J. J. Dannenberg, S. Dapprich, A. D. Daniels, Ö. Farkas, J. B. Foresman, J. V. Ortiz, J. Cioslowski and D. J. Fox, *Journal*, 2009.
86.   R. Stalder, C. Grand, J. Subbiah, F. So and J. R. Reynolds, *Polymer Chemistry*, 2012, **3**, 89-92.
87.   J. Heyd, G. E. Scuseria and M. Ernzerhof, *The Journal of Chemical Physics*, 2003, **118**, 8207-8215.
88.   J. Heyd and G. E. Scuseria, *The Journal of Chemical Physics*, 2004, **121**, 1187-1192.
89.   J. Heyd and G. E. Scuseria, *The Journal of Chemical Physics*, 2004, **120**, 7274-7280.
90.   B. M. Wong and J. G. Cordaro, *The Journal of Physical Chemistry C*, 2011, **115**, 18333-18341.
91.   T. Yanai, D. P. Tew and N. C. Handy, *Chemical Physics Letters*, 2004, **393**, 51-57.
92.   J. Zhang, H.-B. Li, S.-L. Sun, Y. Geng, Y. Wu and Z.-M. Su, *Journal of Materials Chemistry*, 2012, **22**, 568-576.